THESIS OF PHILOSOPHICAL DOCTOR DEGREE

Spectroscopic Studies of the Negative State of Atoms

JAKOB WELANDER

Department of Physics
UNIVERSITY OF GOTHENBURG
Göteborg, Sweden 2020

Jakob Welander

isbn 978-91-7833-976-1 (print)
isbn 978-91-7833-977-8 (pdf)
Available at: http://hdl.handle.net/2077/64417

Department of Physics
University of Gothenburg
se-412 96 Göteborg, Sweden
Telephone +46 31 772 10 00

Printed by: BrandFactory, Gothenburg, Sweden, 2020

Typeset in XeLaTeX with Times Ten and Akzidenz-Grotesk

Abstract

Negative ions are of fundamental interest in atomic physics due to the enhanced importance of the electron correlation. In this thesis new spectroscopic methods have been developed and then applied to study the nature of atomic negative ions. The demand of experimental development in this field is pronounced due to lack of resonant excitations within the atomic negative ion, which makes conventional spectroscopy methods insufficient. Instead, laser photodetachent spectroscopy has been applied in which an ion absorbs a photon resulting in a break up in a neutral atom and an electron. The research has been performed at the Gothenburg University Negative Ion and Laser LAboratory (GUNILLA) and at ISOLDE, CERN.

The work has widened the utilization of spectroscopy techniques to include radioactive elements. For such studies the Gothenburg ANion Detector for Affinity measurements by Laser Photodetachment (GANDALPH) was developed. Of particular interest here is an experimental determination of the electron affinity of astatine of $EA(At) = 2.415\,78(7)$ eV. This work opens for future work on the spectroscopy of transuranium elements and other artificial elements.

Second, a new type of spectrometer for Photoelectron Angular Distribution (PAD) spectroscopy has been developed. In this spectrometer, called PEARLS (Photo-Electron Angular Resolved Linear Spectrometer), the laser and ion beams are collinearly aligned, which considerably increases the interaction volume. The spectrometer was then used to study the energy dependence of the asymmetry parameter β, for photodetachment of negative phosphorous.

Third, a neutral particle detector for collinear spectroscopy is presented. The target material was graphene coated quartz with transparent properties that outperforms the previously used Indium Tin Oxide (ITO). With graphene coating, the accessible energy range is extended to at least 5.3 eV compared to the earlier limit of 3.7 eV.

Finally, an experimental set-up for state selected detection of the residual atom in the photodetachment process has been developed and commissioned. The set-up has been used to measure the EA of cesium to be $EA(Cs) = 0.471\,612(9)$ eV. This work sets the groundwork for investigation of the validity of Wannier's law for three body particle breakups.

Keywords: Atomic Physics, Photodetachment, Negative Ions, Anions, Laser Photodetachment Spectroscopy, Electron Affinity, ISOLDE, CERN, Radioisotopes, Photo Angular Distributions, Graphene, Electron correlation, Neutral Particle Detection, Wannier's Threshold Law.

Preface

With this thesis I want to give a glimpse of the world of quantum mechanics from the perspective of atomic physics and more specifically through the research field of laser spectroscopy of atomic negative ions. The text approaches the subject from an experimentalist´s point of view, although it starts with a brief introduction to the field and its applications in Chapter 1. Chapter 2 is a short introduction to the theoretical foundation of negative ions, and also contains a discussion of the concept of Laser Photodetachment Threshold spectroscopy, which works as a bridge over to the experimental overview in Chapter 3. In Chapter 4 the experimental results, which are presented in detail in the appended papers, are summarized. Chapter 5, finally, gives a conclusion and presents future plans.

Acknowledgements

I can't stress enough that the papers presented in this thesis and the work described in it, is by no means a single mans work. All is the result of team efforts where every single author should have their share of the credit. In addition to the names in the authors lists of the papers I present here a separate list to give my special gratitude to important people, coauthors or not. I have sincerely tried to make my list as comprehensive as possible to include everyone, without any ranking of importance.

Thank you all!

- Anton and Johan for teaching me my first set of skills in laboratory work and showing me the beauty (and frustration) of experimental physics.
- Jan-Åke for supplying parts and long flip passes.
- Mats for sharing your knowledge and your practical support.

- David, Sebastian and rest of Gandalph team
- Jessica for placing the honeycomb on the glass and Avgust for providing it.
- Ademir, Julia and Annie and all the people of the group
- Anders and Martin for sharing the LaTeX-template for this thesis.
- The Swedish tax payers and the Swedish Research Council for giving me the opportunity to contribute to fundamental research and being a part of an inspiring working environment.
- My examiner Raimund and all of the department of physics at the University of Gothenburg.
- Remi and Sten for being a theoretical support when my memory fails to remember the content of the quantum mechanics graduate courses.
- Olle for sharing office and my frustrations of the lab that does not always cooperate. Also for never declining an invitation for a coffee brake with "fika".
- Ludi for showing up at the right time to organize the lab and for sharing your good mood and food recipes.
- Oskar and Andreas for the supporting me to cope with the tear between work and the family.
- Dag for providing the complete support. Second, for acknowledging the greatness in the diversity of your colleague as well as of your students.
- Mum and dad and Johanna for caring, PhD work or not.
- Maja, Love, Elton och Ally för ni alltid frågar: "När är du klar?" Jag lovar att jag är klar när ni läser detta. Då kan vi åka och bada i Rörvik.
- Emma, for being my most critical reviewer and pushing me to be a better me. Your opinion is what matter the most. Love you!

Jakob Welander
Göteborg
12th August, 2020

List of publications

This thesis consists of an introductory text and the following papers:

I **"A graphene-based neutral particle detector"**

J. Warbinek[1,2], D. Leimbach[1,2,3], D. Lu[2], K. Wendt[1], D.J. Pegg[4], A. Yurgens[5], D. Hanstorp[2], J. Welander[2].

[1]Institut für Physik, Johannes Gutenberg-Universität, Mainz, Germany
[2]Department of Physics, University of Gothenburg SE-412 96 Gothenburg, Sweden
[3]CERN, Geneva, Switzerland
[4]Department of Physics, University of Tennessee, Knoxville, Tennessee 37996, USA
[5]Department of Microtechnology and Nanoscience, Chalmers University Technology, SE-41296 Gothenburg, Sweden

Published by: *Appl. Phys. Lett.*, vol. 114,p. 061 902, 2019, DOI: 10.1063/1.5080517.

II **"Laser photodetachment of radioactive $^{128}I^-$"**

Sebastian Rothe[1,2,3], Julia Sundberg[1,2], Jakob Welander[2], Katerina Chrysalidis[1,4], Thomas Day Goodacre[1,3], Valentin Fedosseev[1], Spyridon Fiotakis[1], Oliver Forstner[5], Reinhard Heinke[4], Karl Johnston[1], Tobias Kron[4], Ulli Köster[6], Yuan Liu[7], Bruce Marsh[1], Annie Ringvall-Moberg[1,2], Ralf Erik Rossel[1,4], Christoph Seiffert[1], Dominik Studer[4], Klaus Wendt[4] and Dag Hanstorp[2].

[1] Engineering Department, CERN, Geneva, Switzerland
[2] Department of Physics, Gothenburg University, Gothenburg, Sweden
[3] School of Physics and Astronomy, The University of Manchester, Manchester, UK
[4] Institut für Physik, Johannes Gutenberg-Universität, Mainz, Germany
[5] Friedrich Schiller Universität, Jena, Germany
[6] Institut Laue-Langevin (ILL), Grenoble, France
[7] Physics Division, Oak Ridge National Laboratory (ORNL), Oak Ridge, Tennessee, USA

Published by: *J. Phys. G Nucl. Part. Phys.*, vol. 44,p. 104 003, 2017, DOI: 10.1088/1361-6471/aa80aa.

III **"The electron affinity of astatine"**

David Leimbach[1,2,3], Julia Karls[2], Yangyang Guo[4], Rizwan Ahmed[5], Jochen Ballof[1,6], Lars Bengtsson[2], Ferran Boix Pamies[1], Anastasia Borschevsky[4], Katerina Chrysalidis[1,3], Ephraim Eliav[11], Dmitry Fedorov[7], Valentin Fedosseev[1], Oliver Forstner[8,9], Nicolas Galland[10], Ronald Fernando Garcia Ruiz[1], Camilo Granados[1], Reinhard Heinke[3], Karl Johnston[1], Agota Koszorus[1], Ulli Köster[13], Moa K. Kristiansson[14], Yuan Liu[15], Bruce Marsh[1], Pavel Molkanov[7], Lukáš F. Pašteka[12], Joao Pedro Ramos[1], Eric Renault[10], Mikael Reponen[16], Annie Ringvall-Moberg[1,2], Ralf Erik Rossel[1], Dominik Studer[3], Adam Vernon[17], Jessica Warbinek[2,3], Jakob Welander[2], Klaus Wendt[3], Shane Wilkins[1], Dag Hanstorp[2] and Sebastian Rothe[1]

[1] Engineering Department, CERN, Geneva, Switzerland
[2] Department of Physics, Gothenburg University, Gothenburg, Sweden
[3] Institut für Physik, Johannes Gutenberg-Universität, Mainz, Germany
[4] Van Swinderen Institute for Particle Physics and Gravity, University of Groningen, Groningen, The Netherlands
[5] National Centre for Physics (NCP), Islamabad, Pakistan
[6] Institut für Kernchemie, Johannes Gutenberg-Universita Mainz, Germany
[7] Petersburg Nuclear Physics Institute - NRC KI, Gatchina, Russia
[8] Institut für Optik und Quantenelektronik, Friedrich-Schiller-Universität Jena, Germany
[9] Helmholtz-Institut Jena, Jena, Germany
[10] CEISAM, Université de Nantes, CNRS, Nantes, France
[11] School of Chemistry, Tel Aviv University, Tel Aviv, Israel
[12] Department of Physical and Theoretical Chemistry & Laboratory for Advanced Materials, Faculty of Natural Sciences, Comenius University, Bratislava, Slovakia
[13] Institut Laue-Langevin (ILL), Grenoble, France
[14] Department of Physics, Stockholm University, Stockholm, Sweden
[15] Physics Division, Oak Ridge National Laboratory, Oak Ridge, Tennessee, USA
[16] Department of Physics, University of Jyväskylä, Jyväskylä, Finland
[17] School of Physics and Astronomy, The University of Manchester, Manchester, UK

Published by: *Nat. Commun.*, vol. 11,p. 3824, 2020, DOI: 10.1038/s41467-020-17599-2.

IV **"A collinear angle-resolved photoelectron spectrometer"**

O. Windelius[1,2], A. Aguilar[2], R.C. Bilodeau[2,4], A.M. Juarez[5], I. Rebolledo-Salgado[5], D.J. Pegg[6], J. Rohlén[3], T. Castel[7], J. Welander[3], D. Hanstorp[3].

[1]Department of Physics, Chalmers University of Technology, SE-41296 Gothenburg, Sweden

[2]Advanced Light Source, Lawrence Berkeley National Laboratory, Berkeley, CA 94720, USA
[3]Department of Physics, University of Gothenburg, SE-41296 Gothenburg, Sweden
[4]Department of Physics, University of Connecticut, Storrs, CT 06269
[5]Instituto de Ciencias Fisicas, Universidad Nacional Autonoma de Mexico, PO Box 48-3, Cuernavaca 62251, Mor. Mexico
[6]Department of Physics, University of Tennessee, Knoxville, Tennessee 37996, USA
[7]École Nationale Supérieure d'Ingénieurs de Caen, ENSICAEN 6 Boulevard Maréchal Juin 14050 Caen, France

Published by: *Nucl. Instruments Methods Phys. Res. Sect. B Beam Interact. with Mater. Atoms*, vol. 410,pp. 144–152, 2017, DOI: 10.1016/j.nimb.2017.08.028.

V **"Photoelectron Angular Distributions in Photodetachment from P^-"**

O. Windelius[1,2], J. Welander[1], A. Aleman[1], D.J. Pegg[3], K. V. Jayaprasad[4], S. Ali[5], D. Hanstorp[1].

[1]Department of Physics, University of Gothenburg, SE-412 96 Gothenburg, Sweden
[2]Department of Physics, Chalmers University of Technology, SE-412 96 Gothenburg, Sweden
[3]Department of Physics, University of Tennessee, Knoxville, Tennessee 37996, USA
[4]Department of Physics, University of Gujrat, Jalalpur Jattan Road, Gujrat, 50700, Pakistan
[5]International School of Photonics, Cochin University of Science and Technology, Kalamassery, Kochi-682022, Kerala, India

In Manuscript.

VI **"A Field Ionizer for Photodetachment Studies of Negative Ions"**

J. Welander[1], J. E. Navarro Navarrete[1,2], J. Rohlén[1], T. Leopold[1,3], R. D. Thomas[4], D.J. Pegg[5] and D. Hanstorp[1].

[1]Department of Physics, University of Gothenburg, SE-412 96
[2]Also at: University of Southern Denmark, DK-5230 Odense M
[4]Department of Physics, AlbaNova, Stockholm University, SE-106 91 Stockholm, Sweden
[5]Department of Physics, University of Tennessee, Knoxville, TN 37996, USA

In Manuscript.

Specification of my contributions

I "A graphene-based neutral particle detector"

The idea of this work was proposed during a discussion between me and my supervisor. The main author, J. Warbinek, has performed the actual experiments under my supervision. I was responsible for GUNILLA, with the ion beam facility and the operation of lasers for the experiment. The manuscript was written by the first author and then jointly improved by all co-authors.

II "Laser photodetachment of radioactive $^{128}I^-$"

I took part in preparatory work of the experimental apparatus, partly at the GUNILLA facility in Gothenburg and partly at CERN, Geneva. I took part in the experiment. I am one of the main contributors to the manuscript, particularly in terms of providing the data analysis and preparing the data for the paper.

III "The electron affinity of astatine"

My work efforts for this paper are divided in two parts. First, I took part in the work to commission GANDALPH at the ISOLDE facility at CERN. I took part in all aspects of that work, where my main responsibility was to arrange the data collection system of the two particle detectors. Second, I supported the work of analyzing the data.

IV "A collinear angle-resolved photoelectron spectrometer"

I participated in the experimental work at the GUNILLA facility during experimental runs. I am one of the four authors who contributed to writing the manuscript.

V "Photoelectron Angular Distributions in Photodetachment from P^-"

I participated in the experimental work and took part in the analysis of the data in collaboration with the main author of the paper, O. Windelius. I'm the corresponding author of the paper responsible for the completion of the manuscript in its final form.

VI "A Field Ionizer for Photodetachment Studies of Negative Ions"

The spectrometer was constructed by T. Leopold and J. Rohlén at the GUNILLA facility. I was leading the experimental work to test its performance. The measurement of the threshold data was conducted by J. Navarrate under my supervision. J. Rohlén and myself performed the simulations. J. Rohlén wrote the first version of the manuscript that only contained the simulations. I was the leading author in the final version of the paper that also included the experimental work.

Contents

1

Introduction

Atomic physics was born with the idea of an indivisible particle that builds up matter and runs back to ancient Greece [7].The word atom originates form the greek word atomon, that could be translated to indivisible [8]. The true breakthrough of the research of atomic physics came with understanding the construction of the atom from the results of Rutherford's [9], [10] famous scattering experiment of alpha particles off a thin gold foil. The results were used to create an atomic model with a dense nucleus of positive charge surrounded by a cloud of electrons. With this in hand Niels Bohr created his famous atomic model which successfully was used to explain the quantized energy levels of single electron atomic systems [11]. This was a major step in the creation of quantum physics which successfully has been applied to describe the properties of matter on the atomic scale [12].

In 1913 [13] Thomson[1] identified and listed various charge states of matter as negatively charged electron and positively and negatively charged atoms and molecules. Since this early research negative ions, or anions, have proven to be of fundamental importance. In many examples from daily life or in nature, negative ions appear just as common as positive ions. As an example, sodium chloride ($NaCl$), the composition of ordinary table salt, when dissolved in water, creates salt water with equal amounts of positive Na^+ ions as negative Cl^- ions. Equal amount of charges may also be found in the flame of a candlelight, in a lightning, in the ionosphere or in the magnetosphere [15]–[17]. These are all examples of plasmas, a state of matter defined as a compound of particles of different polarities. However, in atomic physics the situation is quite different. Positive ions can easily be created by supplying sufficient energy to an atom in order to remove one or more electrons. The required energy can be supplied by a projectile particle or a

[1]Most known from discovering the electron in 1897 [14] which granted him the Nobel prize in 1906.

photon. A negative ion, on the other hand, is created by binding an extra electron to a neutral atom, but there is no long range force attracting the negatively charged electron to the neutral atom. However, negative ions can exist if the electrons in the ion move in such a way that they can share the attractive force of the nucleus. This makes atomic anions an interesting construction and a field of its own in atom physics physics. Simply by measuring the binding energy of an anion, the electron affinity (EA), one reveals fundamental quantum principles of the system.

Atomic systems are usually treated theoretically by first assuming that each electron is moving in the average potential created by all other electrons. This is called the Hartee-Fock model [18], and can usually give an accurate basic description of the system. The electron-correlation, i.e. the direct interaction between the electrons, is thereafter added as a perturbation. This procedure, however, is usually not applicable for a negative ion since the Hartee-Fock model many times is unable to predict a stable negative ion. The electron correlation therefore have to be built in to the basic model used to describe a negative ion. Hence, negative ions are suitable systems to benchmark theoretical models ability to incorporate electron correlation. On the other hand, a very simple theoretical description of the anion can be obtained using the "particle in a box model". This model can be used to understand some basic features of anions such as their lack of bound excited states [19].

Negative ions play an important role in many areas of applied research. The discrepancy between the apparent and actual temperature of our sun, has been explained by negative hydrogen ions [20], [21] absorbing and reradiating light in the outer atmosphere of the sun. An equivalent effect is responsible for the opacity of the atmosphere of the earth as well as in the interstellar medium [22]–[24]. However, it's difficult to determine the concentration of anions in these media. This stems from the fact that interaction with light exclusively separates the extra electron from anions due to its lack of bound excited states. Subsequently, anions don't leave any sharp spectral lines as when light interacts with atoms or positive ions. Nevertheless it is of great importance in modeling astrophysical environments to know the basic properties of negative ions and how they interact with other particles. Therefore, negative ions have evolved to be an important topic in the field of laboratory astrophysics [24].

A very important step in atomic physics was the development of laser cooling, for which Steven Chu, Claude Cohen-Tannoudji and William D. Phillips were awarded the 1998 Nobel prize [25]–[27]. This allows detailed studies of atomic systems as the thermal motion which gives a Doppler broadening of atomic lines, is reduced to a negligible level. This opened up the research field, allowing new effects to be investigated. Most striking is the creation of a Bose-Einstein condensate, for which Eric Cornell, Wolfgang Ketterle and Carl Wieman were awarded the Nobel Prize in 2001 [28], [29]. In order to laser cool a system a suitable atomic

transition needs to be found. For positive ions, efficient laser cooling has been achieved for some ions, such as strontium [30]. Here the interesting technique of sympathetic cooling has been developed. By trapping laser cooled Sr^+ ions and with for instance H^+ ions in a trap, the H^+ ions are also cooled through the Coulomb interaction between the cold Sr^+ ions and the hot H^+ ions. In this way any atomic or molecular positive ion can be cooled [31].

Ever since the demonstration of sympathetic cooling of positive ions, the research community has searched for a suitable negative ion to achieve the same effect. For negative ions the situation is not so favorable, since lanthanum [32], cerium [33], osmium [34], and latest discovered thorium [35], are the only species of atomic negative ions where both odd and even parity states have been observed. An alternative would be to use a molecule, where C_2^- is a candidate [36] for laser cooling of negative ions. Research is currently ongoing with the aim to identify a laser transition in one of these elements that can be used for cooling. Finding such a transition would be of great importance since it would open up for cooling of any negative ion. This would, for instance be used to study molecular negative ions that are expected to exist in the cold interstellar medium [37], [38]. The most important application would be to cool anti-protons. Sympathetic cooling of anti-protons requires negative ions as a buffer gas since the anti-protons would immediately merge and annihilate if positive ions were used. By cooling anti-protons it will be possible to more efficiently produce anti-hydrogen. Spectroscopic studies of anti-hydrogen is of great interest since it will reveal information about the symmetry of matter [39].

Spectroscopy, in general, is the experimental tool for atomic physic research. The very first spectroscopic investigations of negative ions were performed using electron impact spectroscopy and polar dissociation spectroscopy [40]. The standard today is to utilize photodetachment where lasers are used as monochromatic light sources giving a method with a high resolution. However, the first known photodetachment experiments were performed with a mercury discharge lamp by Branscomb [41], [42]. Later, the same technique was refined with lasers and therefore came to be known as Laser Photodetachment Electron Spectroscopy [43]. The setup utilizes the narrow linewidth and high intensity of lasers. However, it suffers from a limited resolution of the electron energy analyzing spectrometer. Laser photodetachment threshold spectroscopy (LPT) [44], circumvents this limitation by instead detecting the neutralized atom. Observing the onset of detected atoms while tuning the laser photon energy correlates directly to the EA of the anion. Another method is called Laser Photodetachment Threshold Microscopy [45] where again the detached electron is captured in a conservative field that guides the electron onto an imaging detector which records an interference pattern yielding information about the kinetic energy of the electron. Followed by a rather straightforward subtraction of the kinetic energy from the photon energy one re-

trieves the threshold energy for the photodetachment process. This has proven to be an effective technique, which to date has given the most precise measurements of the electron affinity [46]–[48].

Increasing the photon energy way above the first threshold will eventually open new thresholds or channels of photodetachment. The channel openings corresponds to excitation levels of the residual atom of the photodetachment process. At these energies the photodetachment process is strongly influenced by polarizing effects and resonant behaviours caused by electron-electron interactions, or in other words electron correlation. Many experimental investigations have given new insight of the complexity of the seemingly simple system of the anion [49], [50]. Increasing the energy further will ultimately reach the ionization limit with a double escape of electrons, usually described as double detachment. Many observations of double detachment has been reported, using high energy photon sources [51], [52] or intense laser fields utilizing multi photon absorption [53], [54]. Studies of double detachment has for more than half a century caught attention of theoreticians [55]–[57] since the initial prediction of the threshold behaviour by Wannier in 1953 [58]. Several experiments has been performed [59], [60], although non, to my knowledge, has been able to conclusively distinguish the different theories.

An important method in chemistry [61] is Photoelectron Angular Distributions [62], [63], in which one map out the angular dependence of the escaping electronic wave in the photodetachment or photoionization processes. The PAD of molecules [64] involves rather complicated modelling for the complex composition of molecular orbitals. PAD spectroscopy by photodetachment of atomic negative ions includes, on the other hand, only one electronic orbital. This reduces the possible contributions to the outgoing photoelectron wave and works perfect as a test-bench system for PAD. The most adopted technique for PAD is Velocity Map Imaging (VMI) [65], [66] where the photoelectrons are guided by an electric field on to a position sensitive detector. The geometry of the VMI setup may vary [67], [68] but all have in common that the relative velocity of the emitted electrons creates an image on the detector. The image can therefore be translated back to the original outgoing electron wave.

DESIREE [69], [70] at Stockholm University and CSR [71], [72] at the Max Planck Institute in Heidelberg have recently developed electrostatic storage rings for ions. Both have vacuum conditions of $<10^{-13}$ mbar which reduces collisional detachment allowing storage of ions up to hours. Lifetime measurements of excited states [73], [74] of anions may be performed by probing the population of excited anions using photodetachment while they are decaying to the ground state by spontaneous emission. Further, the long storage time allows for depletion of the population in excited states using a high intensity laser. This can be used to prepare an ensemble of anions that are solely in the ground state. The purified beam of ground state anions combined with continuous wave lasers with bandwidths of

the order of MHz opens up for EA measurements of unrivaled precision [75].

Since Thomson [13] and colleagues of his time initiated mass spectrometry, the field has gone through large developments. One offspring is radiochronometry, maybe most known for its carbon dating method for age determination of anthropological objects. In carbon dating the ratio of ^{12}C and ^{14}C in a sample is determined for which accelerator mass spectroscopy (AMS) is the most sensitive method. In most cases of radiochronometry there is a stable isotope with the same mass as the radiochronometer that gives an experimental background. A method for suppressing such isobaric backgrounds using photodetachment has recently been developed [76], [77]. The ion beam is passed through a radio frequency slower prior to the injection into a tandem accelerator. Here the ion beam is illuminated with laser light that photodetach the interference while leaving the radioisotope unaffected. This is for instance the case when detecting ^{36}Cl in the presence of ^{36}S [78]. In cases where the EA of the interference is larger than the radioisotope, a molecule could be used, as in the case of detecting ^{182}Hf in the presence of ^{182}W, where the $^{182}HfF_5$ is used [79].

Another application of anions is fusion reactors at facilities such as ITER [80]. The current model of fusion reactors rely on a large flux of a neutral beam of deuterium in order to heat the plasma. One promising realization [81] of the high flux neutral beam is by photodetachment of a negative deuterium ion beam.

To conclude, there is a general scientific interest in negative ions. There is now a basic understanding of their properties, but still there are many things to learn. Their unique properties make them ideal systems to test atomic theories that fully include electron correlation. Further, their relative simple structures, where many negative ions only have a single bound state, makes them suitable model systems for investigations of atomic and molecular processes. Further, there are many applications of negative ions where detailed knowledge about the properties of negative ions are required. Hence, there is a demand both to conduct new detailed investigations of negative ions and to develop methods that are more sensitive and yield an improved resolution.

The work presented in this thesis has its focus on improving the experimental techniques. The new experimental techniques include an angular photoelectron spectrometer, a set-up for using resonances ionization spectroscopy for measuring partial photodetachment cross sections and detector for fast neutral atoms that can be combined with UV laser light. The technical development is accompanied with proof-of-principle experiments where the results are of interest both within the field of atomic physics and for applications in other research areas.

The thesis starts with a theoretical background of atomic physics and light-matter interaction and proceeds with an exposition of experimental implementations in the experimental approach chapter. The result chapter is a summary of the experimental findings that are described in detail in the appended papers. The conclusion

and outlook aims to summarize the work and make a projection to the future.

2 Theory

The ideas of Niels Bohr in the early 20th century [11], [82], [83] opened a new era in physics where the classical picture of mechanics on the microscopic scale was replaced with the theory of quantum mechanics. Bohr's ideas were followed up by the French physicist Louis de Broglie who introduced the hypothesis of the wave property of matter where $\lambda = \frac{h}{p}$ [84]. Here λ is the wavelength of a particle of matter, p its momentum and h Planck's constant. Although widely debated in the early days of quantum mechanics, this is today the theoretical foundation for many fields of physics and the indisputable model applied in atomic physics.

The findings of quantum mechanics contradicts the previous intuitive picture that it is possible to simultaneously exactly determine the position and momentum of a particle. This is a consequence of the most fundamental principle of quantum theory, Heisenberg's principle of uncertainty [85], which is a consequence of the wave property of quantum particles[1]. The introduction of the wave function as a solution to the Schrödinger equation [86] brings a method to predict and derive these features. The Schrödinger equation forms the foundation for many fields of physics like condensed matter physics, nuclear physics and atomic physics, all with individual reformulations to describe phenomena specific to the field.

[1]Heisenberg's uncertainty principle can be expressed by, $\Delta r \Delta p = \frac{h}{4\pi}$. It states that it's impossible to simultaneously determine the position and momentum of a particle more accurately than Planck's constant divided by 4π.

2.1 Atomic Physics

2.1.1 Single electron models

One of the first concepts presented in an introductory course in quantum physics is the particle in a box, which is a simple model to describe an electron bound to an atom. Using the Schrödinger equation we can formulate the possible solutions for the electron in a box as

$$\mathcal{H}_{box}\psi_n(\boldsymbol{r},t) = \left[-\frac{\hbar^2}{2m_e}\nabla^2 + V_{box}(\boldsymbol{r})\right]\psi_n(\boldsymbol{r},t) = \frac{d}{dt}\psi_n(\boldsymbol{r},t). \tag{2.1}$$

The solutions to the Schrödinger equation is a set of space and time dependent wave functions $\psi_n(\boldsymbol{r},t)$. For a stationary electron state $\psi_n(\boldsymbol{r},t)$ the time derivative is equal to the quantized eigenenergy E_n. The terms in the square brackets describes the kinetic energy operator and the potential of the box which together form the Hamiltonian operator, $\mathcal{H}_{box}$. The potential of the box is given by

$$V_{box}(\boldsymbol{r}) = 0, \text{ for } \boldsymbol{r} \text{ outside the box and} \tag{2.2}$$
$$V_{box}(\boldsymbol{r}) = -U_0, \text{ for } \boldsymbol{r} \text{ inside the box.} \tag{2.3}$$

The potential of the box and the two wave functions with the lowest energies are illustrated in Figure 2.1. For simplicity the one dimensional case is displayed without the loss of generality when assuming V_{box} to be spherically symmetric. However, as an atomic description the potential of the box is a very simplified model since the electrons in an atom experience a Coulomb $1/r$ potential rather than a constant one. Nevertheless, the particle in a box can be used to illustrate wave functions of a trapped electron and its corresponding quantized eigenenergies.

The single particle model can only be applied in the case of atomic hydrogen and other single electron systems such as He^+, Li^{2+} or U^{91+}. The spherically symmetric Coulomb interaction,

$$V_C(\boldsymbol{r}) = -\frac{e^2}{4\pi\varepsilon_0 r}, \tag{2.4}$$

describes the potential felt by the electron in the hydrogen, where e is the elementary charge, r the radius and ε_0 is the electric susceptibility. The analytically solvable Hamiltonian,

$$\mathcal{H}_{single} = -\frac{\hbar^2}{2m_e}\nabla^2 + V_C, \tag{2.5}$$

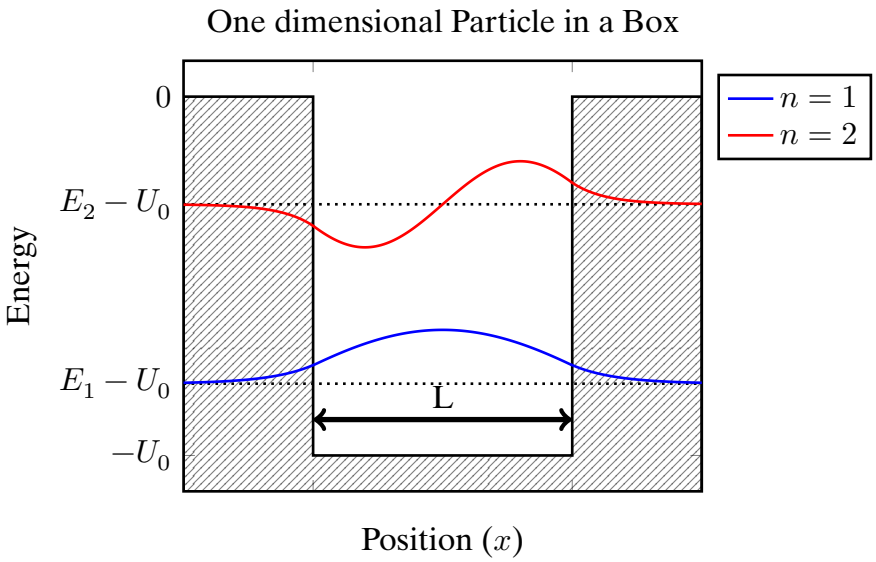

Figure 2.1: The particle in a box model for a one dimensional system with a depth of U_0 and a width of L. The $n = 1, 2$ static wave functions are shown in the figure. The square of the amplitude of the wave function is proportional to possibility to find the particle at a specific location. An important feature to notice is the nonzero probability of finding the particle outside the well, i.e. in an energy forbidden region.

has an infinite number of solutions of state functions ϕ_n with the corresponding eigenenergies

$$E_n = -\frac{m_e e^4}{2(4\pi\varepsilon_0)^2\hbar^2 n^2}, (n = 1, 2, 3, \dots). \tag{2.6}$$

The Hamiltonian in Equation 2.5 may be rewritten in a spherical coordinate formulation with wave functions with separable parts

$$\phi_{n,l,m_l,m_s}(r, \Omega, s) = R_{n,l}(r) Y_{l,m_l}(\Omega) \xi_{m_s}(s). \tag{2.7}$$

Here the radial function $R_{n,l}$, is only dependent on the radial coordinate r. The spherical harmonic function Y_{l,m_l} describes the angular dependence and the spin property is given by ξ_{m_s}. As can be seen from the hydrogenic eigenenergies in Equation 2.6 they're only dependent on the principal quantum number n, while beeing degenerate over l, m_l and m_s[1]. This is a unique property for the spherical symmetry of the hydrogen atom. For all other elements a similar construction

[1]The electron quantum numbers are the principal quantum number n, the orbital quantum number l and its projection m_l and m_s. The latter refers to the spin quantum number which for the electron is fixed, $s = 1/2$. However, its projection, m_s can take both positive or negative values.

of separable wave functions will result in a lifted degeneracy which for example creates the fine structure from the spin-orbit coupling.

2.1.2 Many electron models

For an atomic system of Z electrons where Z denotes the atomic nuclear charge, the interactions can be expressed by the many electron Hamiltonian

$$\mathcal{H} = \sum_{i=1}^{Z} \left(-\frac{\hbar^2}{2m}\nabla_i^2 - Z \cdot V_C(r_i) \right) + \sum_{i<j=1}^{Z} V_C(r_{ij}) - \sum_{i=1}^{Z} \frac{\hbar^2}{2m^2c^2}\frac{1}{r_i}\frac{\partial V_C(r_i)}{\partial r_i}\boldsymbol{l}_i \cdot \boldsymbol{s}_i. \tag{2.8}$$

The first sum is the sum over all electrons, where each term corresponds to the expression of Equation 2.5 for the single electron system. The second sum describes the inter electron Coulomb repulsion and the third sum is the spin-orbit coupling. In practice, this equation is unsolvable unless some simplifications are made. One simplifying approach is the Hartree Fock (HF) approximation where the inter electron repulsion is approximated as a spherical average of the mean field created by all other electrons. The resulting mean field spherical potential may be written as

$$\sum_{i=1}^{Z} U(r_i) = \sum_{i=1}^{Z} -Z \cdot V_C(r_i) + \left\langle \sum_{i<j=1}^{Z} V_C(r_{ij}) \right\rangle. \tag{2.9}$$

This potential makes it possible to construct a hydrogen like Hamiltonian

$$\mathcal{H}_0 = \sum_{i=1}^{Z} -\frac{h^2}{2m}\nabla_i^2 + U(r_i), \tag{2.10}$$

with eigenfunctions constructed from an anti symmetriezed product of hydrogen one electron functions

$$\Psi^{HF}(\boldsymbol{r}_1, \boldsymbol{r}_2, \ldots, \boldsymbol{r}_{\boldsymbol{Z}}) \propto \phi_1(\boldsymbol{r}_1)\phi_2(\boldsymbol{r}_2)\ldots\phi_Z(\boldsymbol{r}_{\boldsymbol{Z}}), \tag{2.11}$$

where the indices of the wave functions denotes a full set of quantum numbers. The details of this antisymmetrized construction are described for instance in the work of Demtröder [87].

The difference between the full Hamiltonian (2.8) and the hydrogen like (2.9) can be expressed as the two terms

$$\mathcal{H}_1 = \sum_{i=1}^{Z} V_C(r_i) - \left\langle \sum_{i<j=1}^{Z} V_C(r_{ij}) \right\rangle \text{ and} \tag{2.12}$$

$$\mathcal{H}_2 = -\sum_{i=1}^{Z} \frac{\hbar^2}{2m^2c^2} \frac{1}{r} \frac{\partial V(r_i)}{\partial r_i} \boldsymbol{l}_i \cdot \boldsymbol{s}_i. \tag{2.13}$$

The size of the terms $\mathcal{H}_1$ and $\mathcal{H}_2$ depends on the atomic system under investigation. The contributions from these two are normally treated as perturbations. By adding these two terms to $\mathcal{H}_0$ one obtains a good approximation of the full Hamiltonian (2.8).

2.1.3 Negative Ions

Negative ions exist despite the fact that a neutral atom and an electron does not have any long range attraction. However, when an extra electron is approaching an atom it will start to perceive the constituents of the atom. The extra electron repels the other electrons of the atom while it is attracted by the positive charge of the nucleus. By slightly pushing the other electrons to the opposite side a net attractive force sufficiently strong to create a negative ion is created. In this way a stable negative ion can be formed for a majority of the elements. This bound state can, just as for atoms, be describe by a wave function to which quantum numbers can be assigned. The lack of a long range attraction of the valence electron contrary to the case of atoms and positive ions leads to a fundamentally different structure of a negative ion. The most striking differences are that the binding energy is about an order of magnitude smaller and that there are only a few, if any, bound excited states. In particular, there are no Rydberg states in negative ions. An example of the energy level diagram of an atom and its negative ion is shown in Figure 2.2.

It turns out that it's very complicated to create a Hamiltonian given by Equation 2.10 that describes a negative ion correctly. A distinct example is the case of hydrogen [88], where a solution to Equation 2.5 gives an unstable system. However, H^- does exist and have an $EA(H^-) = 0.754\,195(19)\,\text{eV}$. Only by using methods including electron correlation resolves this discrepancy. The stability of H^- can, for instance be achieved by applying the Multi Configurational Hartree Fock (MCHF) [89], [90] metod or by using R-matrix calculations [91]–[93].

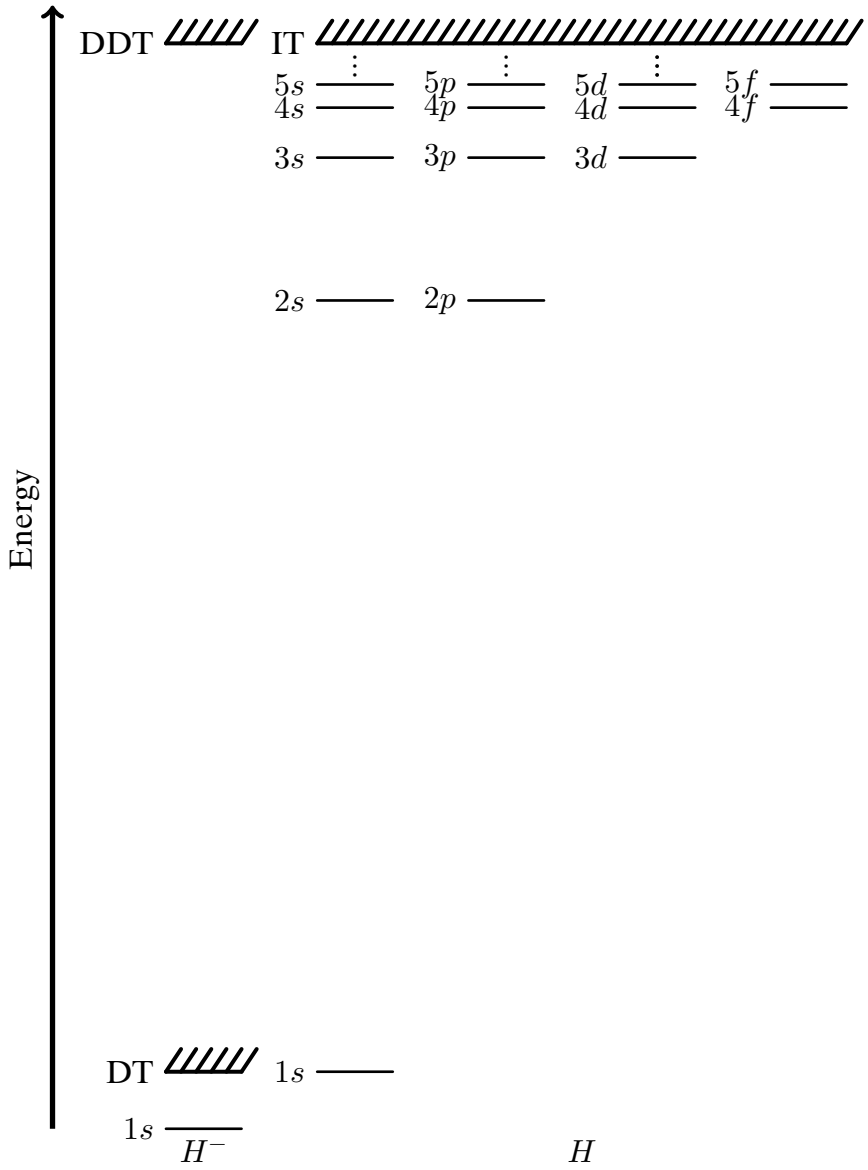

Figure 2.2: The Energy level diagram for hydrogen including the $1s$-state of the negative ion. DT, DDT and IT are abbreviations for detachment, double detachment and ionization thresholds, respectively.

2.2 Light-Matter interaction

Light is interacting with matter all around us and is responsible for most of the fundamental processes that determines the very conditions of life where photosynthesis probably is the most commonly known example. The description of the

light-matter interaction is treated different depending on the scale of the physical system. In atomic physics we're at the quantum scale and the interaction considered is restricted to just a few particles. In this work the light-matter interaction of particular interest is the photodetachment process, where an anion X^- absorbs a photon γ, creating an atom X and a free electron e^-:

$$X^- + \gamma \rightarrow X + e^- \tag{2.14}$$

We can represent this process in terms of energy conservation,

$$E_{GS}(X^-) + h\nu = E_{GS}(X) + K, \tag{2.15}$$

where $E_{GS}(X^-)$ is the ground state energy for the negative ion, $h\nu$ the photon energy, $E_{GS}(X)$ the atomic ground state energy and K is the total kinetic energy of the residual atom and the emitted electron. Due to the conservation of momentum, only a minute fraction, typically of the order of 1‰, of the kinetic energy is taken up by the atom. Hence, the kinetic energy of the outgoing electron, K_{e^-}, can be approximated by

$$K_{e^-} \approx h\nu - EA, \tag{2.16}$$

where we've used the definition of the $EA = E_{GS}(X) - E_{GS}(X^-)$. For photon energies below the EA photodetachment does not occur.

In photodetachment the angular momenta of the emitted electron follow the selection rule,

$$l_{bound} \overset{+}{(-)} 1 = l. \tag{2.17}$$

Here l_{bound} is the angular momentum of the electron prior to photodetachment and l the angular momentum of the outgoing electron. The photon contributes with $\overset{+}{(-)} 1$ under the assumption of the dipole approximation. The minus sign is dropped for the special case of photodetachment of an s electron, which only can be emitted as a p wave. More generally, l is represented by the two solutions to Equation 2.17 where, in particular, photodetachment of a p electron leads to an electron being emitted as a s or d wave.

In the vicinity of the atom, the valence electron still feels the potential energy term described in Equation 2.12. At larger distances the electron experience a potential from the distorted atom that may be approximated by an induced dipole potential expressed by

$$V_{pol}(r) \propto \frac{-\alpha}{2r^4}, \text{ for } r \gg r_0. \tag{2.18}$$

Here r_0 is the radius of the residual atom and α is the atomic polarizability. The polarizability can differ several orders of magnitude between different elements[1]. Further, it increases dramatically, scaling as n^7, for a residual atom left in an excited state in the photodetachment process. The effective potential also depends on the angular momentum l due to the centrifugal force giving a potential described by

$$V_{eff}(\boldsymbol{r}) = V_{pol}(r) + V_l(r) \propto \frac{-\alpha}{2r^4} + \frac{l(l+1)}{2r^2}. \tag{2.19}$$

The effective potential including the so called centrifugal barrier is graphical represented in Figure 2.3 for $l = \{0, 1, 2\}$. As a reference, a Coulomb potential is plotted in the figure. One should point out that V_{eff} is not the true binding

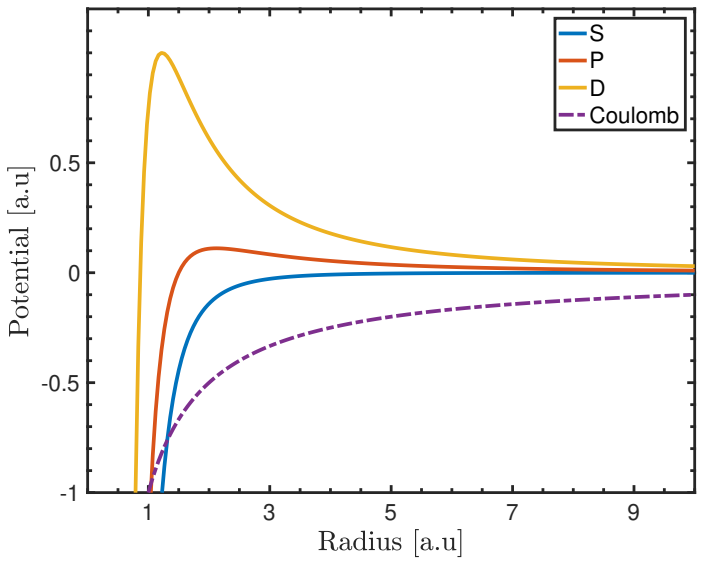

Figure 2.3: A representation of the effective potential of the polarization induced potential and centrifugal barrier. The figure also shows the long range Coulomb potential.

mechanism of the anion, but a simplified model that can be used to understand the photodetachment process. Figure 2.3 shows for photodetachment of an s-electron, detachment can occur as soon as the energy provided by the photon is sufficient to bring up to zero in energy. Also photodetachment of p- and d- electrons can occur, but for lower positive energies the electron has to tunnel through the centrifugal

[1]Although generally positive, interesting cases of negative polarizability for photodetachment from specific orbitals has been discovered [49], [50]. From these findings it's possible to state that the strength (and sign) of the polarization α is a measure of the degree of correlation among the electrons in the anion.

barrier. In the detachment into an s-orbital an intuitive picture can be obtained by comparing with the box potential of Equation 2.2. This simplified process has its graphical representation in Figure 2.4a, where the blue curve represent the wave function of the electron in the negative ion and ψ_1, ψ_2 and ψ_3 represent the wave functions of the emitted electron at three different energies, respectively. The energy cross section of the photodetachment process has been theoretically treated by Amusia [94] who showed that it can be expressed as

$$\sigma_{tot} \propto \sqrt{EA}\frac{\sqrt{(h\nu - EA)^3}}{h^3\nu^3}. \tag{2.20}$$

Figure 2.4b shows the same model of a continuously nonzero cross section curve above threshold. In order to couple Figure 2.4a and 2.4b together, the rest of this section will discuss the resemblance between the two.

Equation 2.20 is graphically shown in Figure 2.4b where the contribution of additional channel openings that modulates the total cross section with overlapping additions and resonant structures has been neglected (See section 2.2.2), nor does it consider the effect of the centrifugal barrier which affects the cross section in the small energy region near the photodetachment threshold. It turns out that one can qualitatively understand the cross section curve shown in Figure 2.4b by some simple arguments based on Figure 2.1. For a photon energy lower than the binding energy ($h\nu_r$) no photodetachment occurs. When the photon energy is slightly larger than the binding energy ($h\nu_g$) it becomes possible to detach the electron. However, the overlap between the wave function of the negative ion (ψ_{bound}) and the tail of the wave of the emitted electron (ψ_1) is in this case small, and hence the cross section is small. As the photon energy increases ($h\nu_b$) the wavelength of the outgoing electron decreases which leads to a larger overlap between the initial and final wave function. Therefore, the cross section increases until it reaches its peak, which as a rule of thumb occurs at $2EA$. This is typically when the wavelength of the outgoing electron corresponds to the size of the potential well. For higher photodetachment energies the free electron wave function (ψ_3) starts to oscillate which leads to a decreasing overlap between the initial wave function (ψ_{bound}) and the final wave function, leading to a cross section that tends towards zero.

2.2.1 The Wigner Threshold Law

Eugene Paul Wigner, a theoretician granted with a Nobel price in 1963 for his contributions to elementary particle and nuclear physics, also provided important findings for the theory of photodetachment. His derivations on the low energy region of two particle break up [95] lead to a highly applicable and valuable tool for experimental analysis of the photodetachment process. As the starting point of

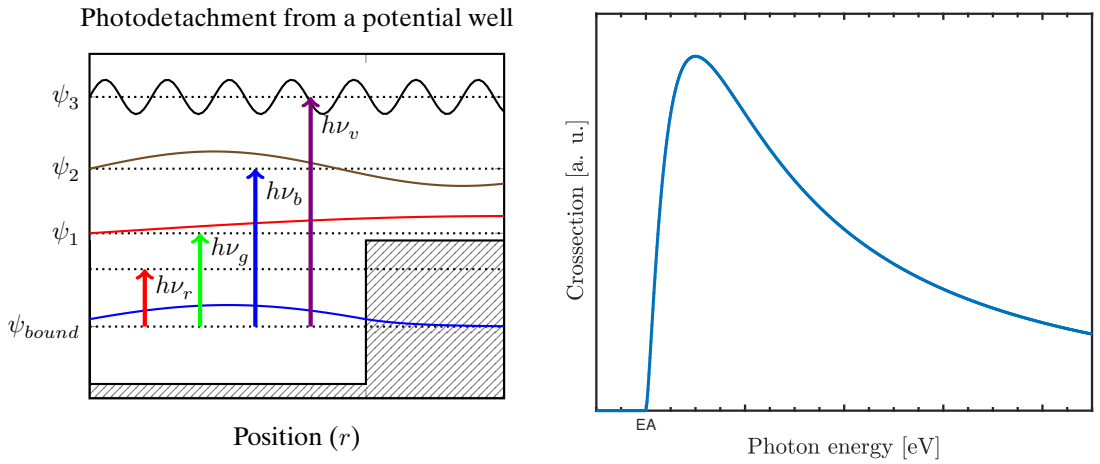

Figure 2.4: Figure (a) shows the photodetachment process of four separate cases of visible photon energies ($h\nu_v$, $h\nu_b$ $h\nu_g$ and $h\nu_r$). The box potential is an approximation which can bee used to qualitatively describe the overall behaviour of the total cross section which is shown in Figure (b). Particularly interesting is the peak value of (b) that coincide with the largest overlap between the initial (ψ_{bound}) and final (ψ_b) wave functions.

the derivation he regards a cross section that only depends on long range interaction potentials of the particle break up irregardless of the origin of the scattering interaction. In the case of photodetachment the short range polarization potential, V_{pol}, in Equation 2.19 is neglected. Instead only the centrifugal barrier affect the cross section. This leads to Wigner's law for cross section near threshold given by the expression

$$\sigma_i \propto (h\nu - EA)^{l_i+1/2}, \text{ for } h\nu \geq EA. \tag{2.21}$$

The exponent of $1/2$ originates from the density of states in the continuum whereas l_i is a consequence of the centrifugal barrier. The difference $h\nu - EA$ determines the total kinetic energy K, shared between the products of the photodetachment process. In Figure the 2.5 Wigner threshold law is shown for the first three partial waves, $l_i = 1, 2, 3$. One can clearly see how the p- and d- waves are suppressed at their thresholds, whereas the s-wave detachment gives an onset that scales as a square root function.

There can be several states involved in a photodetachment process, and each of those state can be split due to fine and/or hyperfine structure. The total threshold

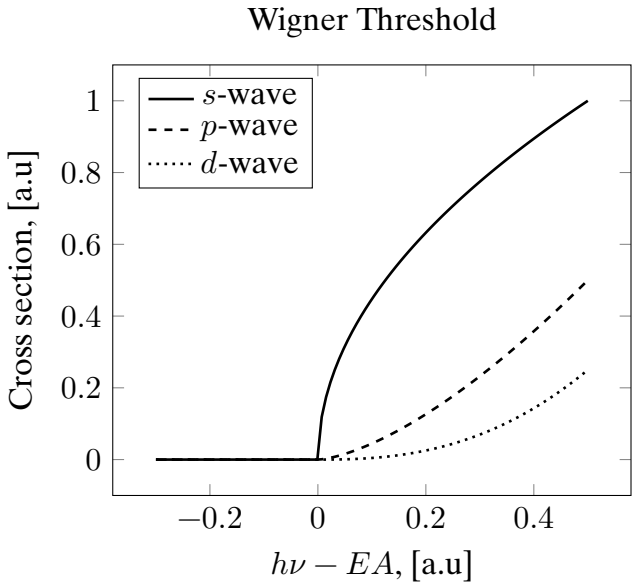

Figure 2.5: Threshold behavior of the photodetachment cross section from each partial wave respectively. All according to the Wigner threshold law of Equation 2.21.

cross section is then expressed by an summation of all contributions,

$$\sigma_W = \sum_i c_i \left(h\nu - (EA + \Delta E_i)\right)^{l_i+1/2} \Theta\left(h\nu - (EA + \Delta E_i)\right) \tag{2.22}$$

The summation over i corresponds to all allowed transitions from initial anion states to final atomic states. EA is defined as energy difference between the ground states of the negative ion and the atom. δE_i are the transitional energy shifts due to the lifted degeneracy and c_i are constants. The Heaviside step function Θ ensures the discontinuity from Equation 2.21 over each channel opening of partial cross section σ_i. One should note that excited bound states close to the threshold with different orbital angular momenta are rare. Hence the value l_i is normally the same for all thresholds that opens in a limited energy range.

A residual atom left in an excited state may experience a higher polarizability during photodetachment and effectively serve as a long range attraction for the detaching electron. This affects the validity of the Wigner threshold law. Instead an alternative formulation of the threshold law including the effect of the polarized atom has been developed by O'Malley [96]. However, for energies far above the threshold region a diversity of photodetachment channels of more exotic nature occur.

2.2.2 Doubly excited states

The concept of resonances occurs in essentially all fields of physics and atomic anions are no exception. Of particular interest in this context are the so called doubly excited states (DES) which was first observed in atomic system in spectroscopic studies of noble gases [97] using the first generation of synchrotron light sources.

The first observation of DESs in negative ions was made by Bryant and coworkers who studied H^- using a relativistic ion beam [98]. These state are formed by a photon absorbing sufficiently amount of energy to excite two electrons. These states can be described by assuming that an excited state in an atom binds an extra electron. The binding energy of such a state with respect to its so called parent state is usually very small. A resonance observed at this energy is usually called a Feshbach resonance. Such a state can decay by one electron returning to a lower state in the atom while the other is emitted. The state could also be situated above the parent state but still being trapped due to the centrifugal barrier. Such a state gives rise to what is called a shape resonance. In this case the system can decay to the parent state by tunneling through the centrifugal barrier. The presence of DES appears as modulations in the total cross section for photodetachment. The phase shift between direct photodetachment and detachment via the DES can be either constructive or destructive. The general expression of such a resonance can be described using the expression derived by Shore [99]:

$$\sigma_{DES} = \sigma_{tot}\left(1 + \frac{\epsilon a + b}{\epsilon^2 + 1}\right). \tag{2.23}$$

Here σ_{tot} is cross section for the direct photodetachment process and the fraction inside the parenthesis is the term causing a modulation. The fractional includes phase parameters a and b and the actual DES dependent parameter $\epsilon = (h\nu - E_{DES})/(\Gamma/2)$, where E_{DES} and Γ are the energy and width of the DES, respectively. The expression of Equation 2.23 is a reformulation of the expression deduced by Fano [100] for such resonances and therefore referred to as Fano profiles.

The amplitude of the resonances are normally very small compared with σ_{tot} and may be hard to discriminate from the background it generates. State selective experiments [101] utilizing partial cross sections σ_i can favourably be used to observe these resonances.

2.2.3 Photoelectron Angular Distributions

Either the neutral atom or the electron can be used to detect the photodetachment process. The total photodetachment cross section σ_{tot} can be measured by

detecting the total yield of neutral atoms or all emitted electrons. Partial photodetachment cross sections be detected either by measuring the energy of the emitted electron or with a state specific detection of the residual atom. By detecting the direction of the emitted electron, finally, the differential cross section $\frac{d\sigma_{tot}}{d\Omega}$ can be determined. The research field in the latter case is referred to as Photoelectron Angular Distributions or PAD in short, where photoelectron refers to the product of photodetachment or from photoionization. The angular dependence of the electron wave from an unpolarized target ion can be described by the formula

$$\sigma_{diff} = \frac{d\sigma_{tot}}{d\Omega} = \frac{\sigma_{tot}}{4\pi}\left(1 + \beta\frac{3\cos^2(\theta) - 1}{2}\right), \text{ for } \beta \in [-1, 2]. \tag{2.24}$$

Here θ refers to the angle between the emitted electron and the polarization of the light which induces the process. β is named the asymmetry parameter. The proportionality constant $\frac{\sigma_{tot}}{4\pi}$ ensures that the total cross section σ_{tot} is obtained under integration over the solid angle. Four special cases of β are particularly interesting. For $\beta = 0$ (Figure 2.6a) we can see that σ_{diff} becomes isotropic. $\beta = 2$ (Figure 2.6b) gives a $\cos^2(\theta)$ dependence which has the form of p-orbital, and $\beta = 1$ (Figure 2.6c) resembles a d-orbital. The most interesting case is $\beta = -1$ where the angular dependence has a $\sin^2(\theta)$ as shown in Figure 2.6d. This distribution cannot be represented with a spherical harmonic. Instead, this distribution can be obtained from a superposition of an s-wave and d-wave including a summation over all magnetic quantum numbers [102].

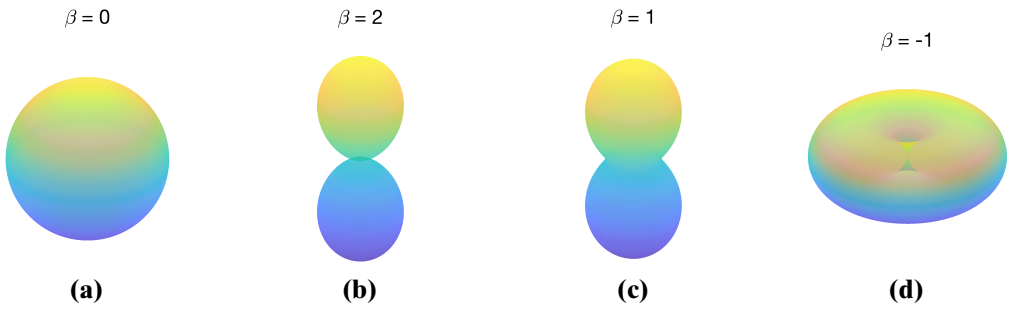

Figure 2.6: A set of angular distributions in 3 dimensions using Eq. 2.24 and completing the azimuthal symmetry. Values of β are displayed for all Figures (a)-(d).

Resolving the physical contributions of PADs is not a trivial task, in particular for molecular systems where the many different emission channels produce very complex distribution. The Cooper-Zare formula was presented in 1968 [62], [63] with the full formulation of the energy dependence of β, computed from transition

matrix elements, $\sigma_{l\pm1}$ of light-ion interaction.

$$\beta = \frac{l(l-1)\sigma_{l-1}^2 + (l+1)(l+2)\sigma_{l+1}^2 - 6l(l+1)\sigma_{l-1}\sigma_{l+1}\cos(\delta_{l+1} - \delta_{l-1})}{(2l+1)\left[l\sigma_{l-1}^2 + (l+1)\sigma_{l+1}^2\right]} \quad (2.25)$$

Here, $\delta_{l\pm1}$ are the phases of the outgoing partial waves which in general is energy dependent. Breaking up the problem in parts, anions is a perfect starting point due to its pure outgoing electron waves following photodetachment. For the case of anionic bound p-state detachment the two mixing contributions of the outgoing electrons have s- and d-character. A model developed by Hanstorp *et al.* [103] successfully recreates the experimental data behaviour of photodetached O^-:

$$\beta = \frac{2A_2\varepsilon(A_2\varepsilon - 2c)}{1 + 2A_2^2\varepsilon^2} \quad (2.26)$$

In this model A_2 and c are the model parameters and ε the energy above the threshold. This model, which is an approximation of the full Cooper-Zare formulation in Equation 2.25, has been shown to be a very powerful experimental tool. The model and its interpretation will be further discussed in Chapter 4.

2.3 EA vs. IE

As discussed earlier in this chapter there's a fundamental difference between the force keeping a negative ion together compared those of atoms or positive ions. The difference could be found more prominent by visual inspection of the EA over the whole periodic table, as presented in Figure 2.7. For the case of the IEs of the elements I do not provide a visual representation. Instead the over all behaviour may as well be summarized in a few statements. The column with lowest IEs are found for the alkaline group, to the far left in the periodic table. This stems from the fact that there's only a single valence electron which is efficiently screened from the attraction of the nucleus by the core electrons. Moving along the columns to the right corresponds to increasing number of electrons in the valence shell. The screening from the valence shell electron are not as efficient as from the core and consequently the effective charge felt by the valence electron becomes larger. This results in increased effective charge giving an increase in the IEs. Francium (Fr) has the smallest IE of all element, which is a consequence of its highest expectation value of the radial distance from the core. The argument can be made for all of the columns of the periodic table. Hence, we find the lowest IE for each column at the bottom of the periodic table. There are few exceptions to these trends where for instance nitrogen (N) has a larger IE than Oxygen (O). Nevertheless, this crude

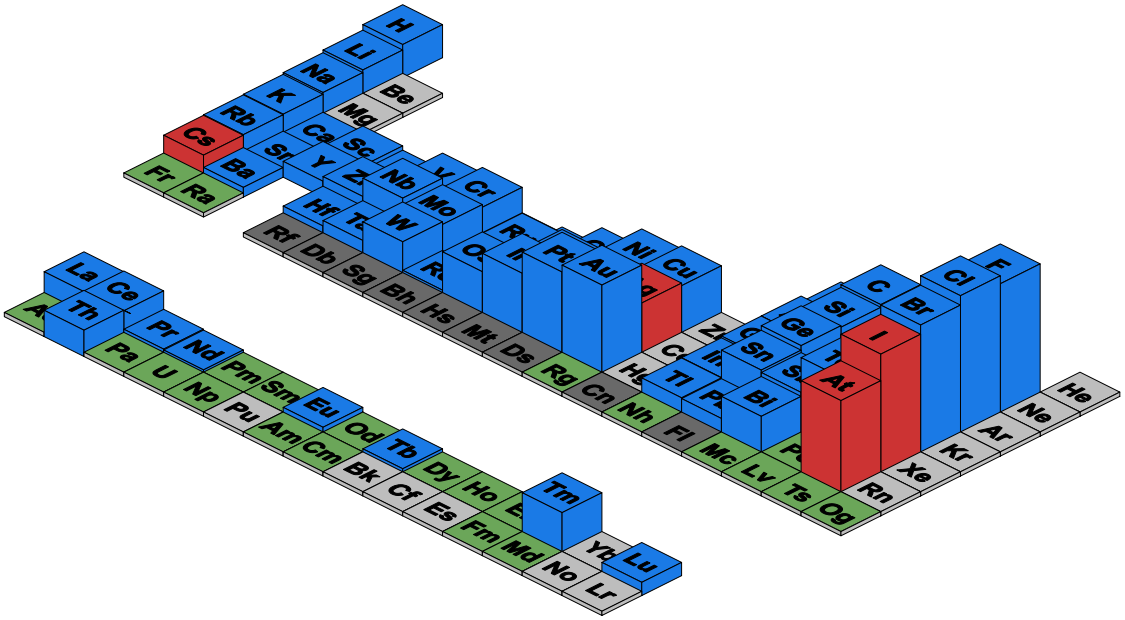

Figure 2.7: The periodic table with the heights of the blue bars corresponding to the EA of the elements. Light grey elements have been determine to have negative EA and hence do not form negative ions. Green elements are theoretically predicted to form negative ions but has not yet been under experimental investigation. Elements that have not been experimentally investigated nor theoretically predicted are dark grey. Red bars belongs to elements under investigation in this work.

model grasps the over all trends quite well. The periodic table of the EA, shows a complete different structure. There are no over all trends that can be described by one general model. Instead it's the details that needs to be under consideration in order to explain the interrelated values of EA between the elements. Off course some fast conclusions can be made from a visual investigation of 2.7. For instance, elements where the parenting atom have electron configurations that forms closed shells or subshells are generally not forming negative ions, where the noble gases and the last column of the transition metals can serve as examples.

3

Experimental approach

In the introduction of this thesis it was described how one can experimentally study negative ions in storage rings, ion traps or in a single pass ion beam apparatus. In this thesis I've used two different single pass ion beam apparatuses for laser photodetachment studies. One was used for investigations of stable negative ions and another one for studies of radioactive isotopes. In both facilities an ion source was attached to an accelerator in order to form an ion beam. Further one needs a mass selective element to purify the beam to a specific element before guiding it to an interaction region. In the interaction region anions interact with photons. Various detectors are used to monitor particle fluxes as well as residual products of the photodetachment process. In the following sections the different parts of the experimental facilities will be described.

3.1 Experimental conditions

A negative ion source can typically be used to create ion currents of the order of pA to nA of a specific element. Intense photon beams are obtained using pulsed lasers with nanosecond pulse widths. A crucial part in photodetachment experiment is to perform it under good vacuum conditions since any experiment is a competition between wanted and unwanted effects. Negative ions created in the ion source can be destroyed by collisions with residual gas. The average distance an ion travels without being destroyed is expressed as the mean free path. Collision with the residual gas also generates background events which competes with the signal events. The transport of an ion beam requires a pressure lower than 10^{-6} mbar and signal to noise levels is reasonable under the conditions of 10^{-8} mbar[1].

[1]Off course highly dependent on the ion and photon fluxes.

3.1.1 Geometrical considerations

Just as for an optical source, an ion source creates a divergent beam determined by the geometrical dimensions of the source. Furthermore, the transport of a beam of ions resembles an optical setup with mirrors and lenses used to manipulate either its path or shape. The possibility to manipulate a beam is described by Liouvilles theorem [104], [105] which in short sets a limitation of its size and divergence. The interaction region for the beams of ions and laser may be restricted for practical reasons but can in principle be constructed with any angle from 0° to 180°. Historically, most experiments have been performed using crossed (90°) or collinear (0°/180°) geometries. Comparing the two, the collinear geometry gives at least two orders of magnitude larger interaction volume. However, the well defined volume of crossed beam setups[1] opens up for precision absolute cross section measurements while the collinear setup typically are used to measure relative cross sections. In a cross beams geometry any deviation from 90° gives a Doppler shift. Hence, the angular spread of the ion and laser beam, even if minute, gives a large Doppler broadening [107]. On the contrary, the divergence of the laser and ion beams in collinear geometry gives a very small Doppler broadening. Further, the Doppler compression reduces the relative velocity spread allowing high resolution experiments [108]. However, a large Doppler shift will occur, but this can easily be compensated for to all orders by measuring with both co- and counter propagating ions and laser beams and calculating the geometrical mean of the results [109].

3.2 GUNILLA

GUNILLA is an acronym for Gothenburg University Negative Ion and Laser LAboratory. It is designed for total cross section measurements, photoelectron angular distribution studies and for detection of Rydberg atoms. A schematic representation of the setup is given in Figure 3.1. A Cesium sputter source which creates the negative ions is placed on the top. A drift region is connecting the source with a mass selective electromagnet. An ion optical Einzel lens and a horizontally aligned one-dimensional lens (not shown in figure) focuses the beam onto an aperture. The aperture defines the object position of the magnet to be imaged on an aperture after a singly focusing magnet. A vertically aligned one-dimensional lens (not shown in figure) positioned between the magnet and the subsequent aperture focuses the vertical part of the beam onto the aperture. The drift region after the magnet houses a quadrupole triplet (not shown in figure), shaping the beam to the desired shape for the spectrometers placed downstream. A single turbo

[1]Crossed beam geometry allows the technique of animated beam [106] to precisely determine the interaction volume of the laser and ion beams.

pump produces the source chamber vacuum of the order of 10^{-6} mbar while the post magnet drift region operates at high 10^{-8} mbar via a turbo pump in combination with dual set of ion pumps. Faraday cups can be slid in behind apertures to measure the ion current before and after being mass selected. Finally, the ion beam is directed into one of three different interaction regions. In Section 3.2.2, the Doppler spectrometer, which can be used to measure total photodetachment cross section is described. PEARLS, described in 3.2.3, is used to measure photoelectron angular distributions, and finally RADAR, presented in section 3.2.4, can be used for detection of Rydberg atoms.

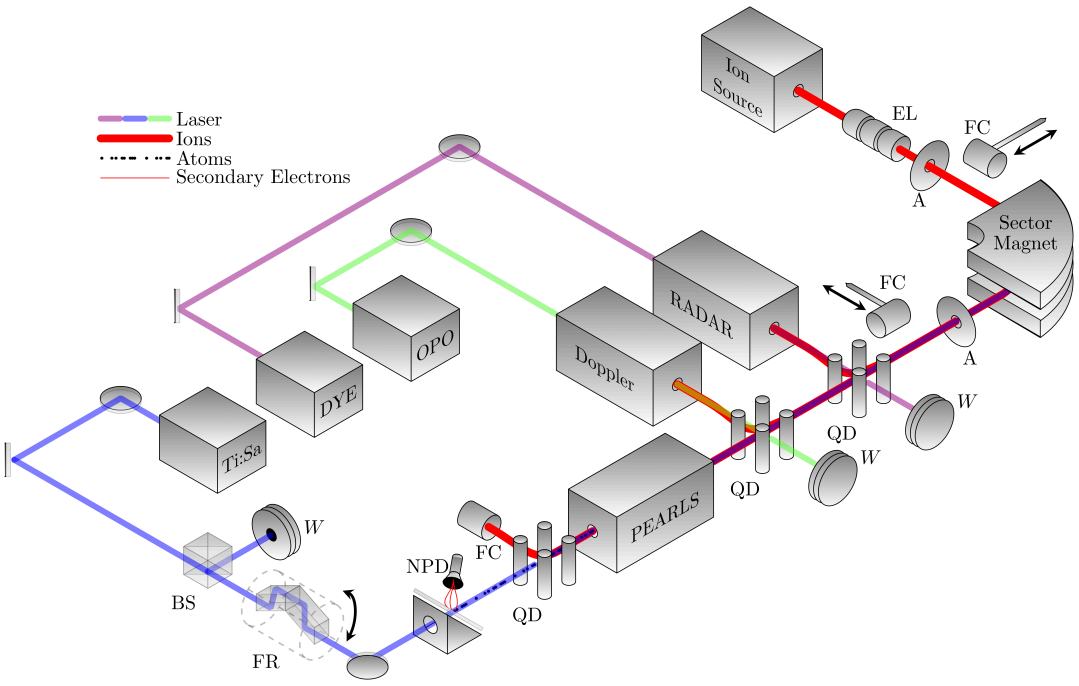

Figure 3.1: The GUNILLA setup starting with the Ion Source and a Mass Selecting magnet. The ion beam can be directed into three different spectrometers - RADAR, Doppler and PEARLS. Laser light is provided by high intensity lasers (Ti:Sa, Dye and OPO). The Einzel lens (EL), Quadrupole Deflectors (QD) and apertures (A) are used to guide and control the ion beam. The Neutral Particle Detector (NPD), Faraday Cups (FC) and Power Meters (W) are beam diagnostic tools in addition to the integrated detectors of the three spectrometers. Lasers are guided by optical mirrors and a Beam Splitter (BS). A Fresnel Romb (FR) is used to rotate the polarization to any chosen angle for PAD experiments using PEARLS.

3.2.1 Cesium Sputter Ion Source

The Ion source of GUNILLA is a PS-120 negative sputter ion source from Peabody Scientific based on the design of Middleton [110]. It utilizes the element of Cesium, which has a very low IE, both as an electron donor and as a sputtering projectile particle on the target material for anion creation. Room temperature cesium is crystalline but melts at 28.5 °C. The cesium is vaporized by heating to temperatures of 100 °C to 150 °C providing a cesium rich environment in the source main chamber. A spherical tantalum[1] surface ionizer which is kept at temperature of over 1300 °C ionizes the cesium atoms by surface ionization. The ions are then accelerated by 3 kV towards the cathode. The cathode contains the target material which is sputtered by the projectile cesium positive ions. The cathode is water cooled in order to condensate the neutral cesium on its surface. Sputtered atoms and molecules will, with a large probability, capture an electron from the condensed cesium in a charge transfer process, hence being converted to negative ions. The negative ions are accelerated towards the ionizer voltage and extracted by an additional electrode placed on ground potential. Consequently, a negative ion beam is directed towards the sector magnet. The typical configuration of the PS-120 at GUNILLA creates a 6 keV ion beam of a few µA before mass selection. The single mass beam after the electromagnet is of the order of hundreds of pA to tens of nA, highly dependent on the target material and the selected element. All elements can be produced in the sputter source besides a few exception such as nitrogen and the noble gases because of their inability to form stable negative ions. No radioactive isotopes are handled at GUNILLA due to safety restrictions.

The source description provided above is highly simplified and does not discuss any crucial mechanisms occurring inside or on the surface of the cathode. Plasma conditions are observed to be involved [114] which leads to a high ion yield. This is a subject of ongoing research within the field of mass spectrometry.

3.2.2 The Doppler Spectrometer

Total photodetachment cross section measurements are performed using the Doppler Spectrometer. An overview of this spectrometer can be seen in Figure 3.2. The negative ion beam is deflected into the spectrometer by means of an electrostatic quadrupole deflector. Two apertures of 3 mm diameter defines a 20 cm interaction region where the ion beam is overlapped with a laser beam. LPT experiments may be performed using light from a tunable laser in a parallel or anti-

[1]The Ta surface on the ionizer has a work function of 4.25 eV [111], [112] which is larger than the ionization energy of Cs 3.9 eV [113]. Hence, an exothermic reaction creates positive cesium ions with almost 100 % efficiency.

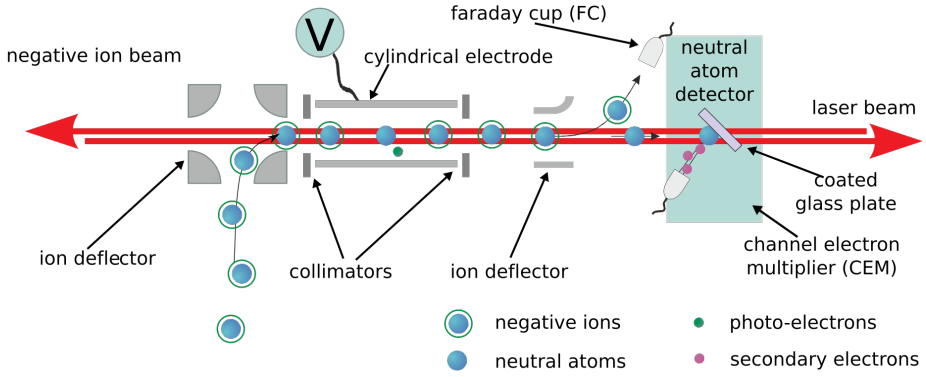

Figure 3.2: Schematic layout of the Doppler spectrometer. A beam of negative ions is overlapped with a laser beam, arranged in either a co- or counter-propagating. The neutral atoms produced in the photodetachment process impinge on a coated glass substrate where secondary electrons are created and detected by a channel electron multiplier. Remaining undetached ions are deflected towards a Faraday cup.

parallel geometry. A pair of deflectors plates separates the residual ions, directed into a Faraday cup, from the neutralized atoms that are detected with neutral particle detector. An additional option for energy scanning is provided by a cylindrical electrode placed between the two apertures. Positive (negative) potential of the electrode provides an addition (subtraction) to the kinetic energy which subsequently increases or decreases the Doppler shift depending on whether a parallel or anti-parallel geometry is used. This added feature explains the name[1] of the spectrometer. The advantage of the Doppler tuning is that there is no need to tune the laser wavelength in a threshold measurement.

The Neutral Particle Detector (NPD) of the Doppler spectrometer is a construction by the design of Hanstorp [115]. The central parts of the NPD is a transparent and conductive plate and a Channel Electron Multiplier (CEM). The transparent plate allows laser light to pass straight through and simultaneously act as a target for neutral impinging particles from the photodetachment process, as seen in Figure 3.3. On impact the neutral particles creates secondary electrons which are collected with the CEM. The multiplication factor of the CEM is of the order of 10^9 times and gives an analogue voltage pulse of a few tens of mV for a single electron detection. The combination of the collection efficiency of the CEM and total emission of 2-3 secondary electron per neutral gives a total detection efficiency of nearly 100 % [115]. Despite the transparency of the glass plate high intensity laser

[1]Christian Doppler was a mathematician and physicist observing stars and related the appearing color to what is known as the Doppler shift due to non zero relative velocity between transmitter and observer.

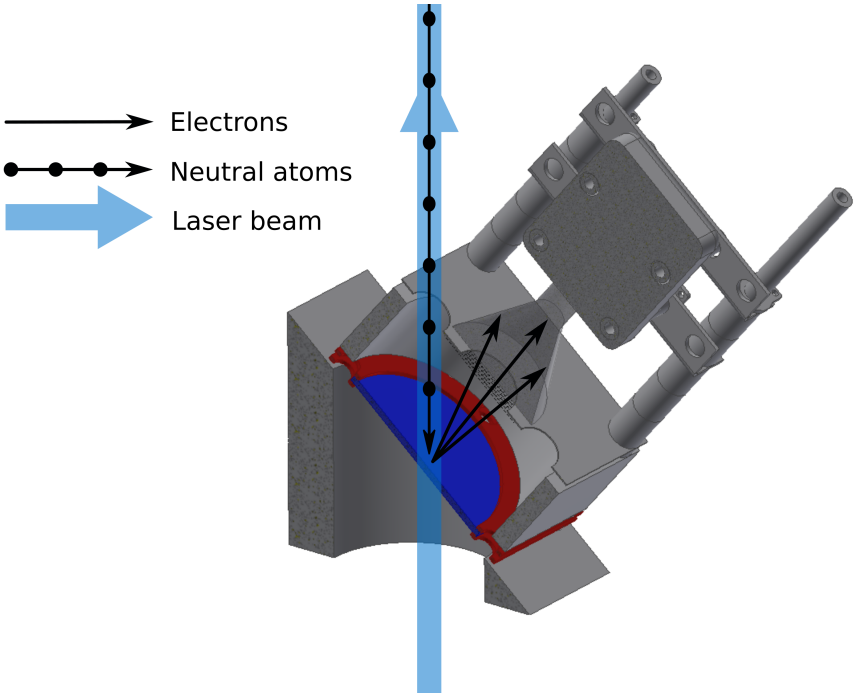

Figure 3.3: From the collinear interaction region ions, atoms and laser are fully overlapped. The ions are deflected by a electric field deflector. Hence, only neutral atoms travel on to the target glass plate. Secondary electrons scatter off the glass plate and are collected by the Channel Electron Multiplier (CEM).

pulses create electrons through the photoelectric effect. For photon energies below the work function of the target material the effect is small since it requires a multiphoton process. For photon energies above the material work function, on the other hand, the effects can be very large and saturate the NPD. In order to suppress interfering photoelectrons a switchable mesh is placed in front of the CEM. The material of the plate is crucial since it needs to be simultaneously transparent and conducting. In the original design, ITO (tin doped indium oxide) on BK7 (standard glass) were used. In the work presented in paper

3.2.3 PEARLS

The Photo Electron Angular-Resolved Linear Spectrometer (PEARLS) is a collinear spectrometer for PAD spectroscopy of atomic and molecular ions using lasers or synchrotrons such as MAX IV [116]. A design view of PEARLS is shown in Figure 3.4. The collinear geometry is defined by two apertures at a 50 cm distance. An FC and an NPD, placed after a deflector separating ions and atoms exiting the interaction region, are included for normalizing purposes (Figure 3.1).

A graphite tube surrounds the interaction region where 4 lines of holes have been drilled along the tube. 16 CEMs are positioned such that they detect electrons that have passed through the holes. The setup of CEM detectors are designed to simultaneous collect photodetached electrons in four perpendicular directions. This makes it possible to map to the total 4π emission of the outgoing electron wave by determining the ratio of two perpendicular positioned detectors

$$C = \frac{\sigma_{diff}(90)}{\sigma_{diff}(0)}. \tag{3.1}$$

As described in Paper IV the asymmetry parameter β can then be deduced by the expression.

$$\beta = \frac{1 - C}{1 + C/2} \tag{3.2}$$

A PAD study may vary in complexity depending on the system under investigation. Anions with photon energy dependent angular distribution are of particular interest. A complication occurs if the photon energies are sufficient to leave the residual atom in an excited state, or if an excited state of the anion is populated. In this case the electrons of different detachment channels will have different energies. For this reason, electrodes are placed at the exit holes of the tube and serves as an energy high pass filter to suppress low energetic electrons.

3.2.4 RADAR

Photodetachment can occur as soon as the photon energy is larger than the EA of the negative ion under investigation. By the principle of angular momentum conservation, the initial and final state of the photodetachment determines the possible angular momenta of the outgoing electronic wave. The onset of photodetachment events above threshold depends on the angular momentum according to Wigner's threshold law [95] described in Section 2.2.1. As seen from Equation 2.21 and Figure 2.5, an outgoing electron with an angular momentum larger than 1 gives an onset which is less pronounced and therefore harder to determine experimentally. This fact makes for instance the halogens ideal for high precision LPT measurements. On the other hand, photodetachment from the alkali metals instead gives a slow onset. Two-photon energy experiment has been conducted at GUNILLA in earlier work [49], [50]. In these studies photodetachment with photon energies sufficiently high to open the possibility to leave the residual atom in an excited state. These channel openings adds extra contributions to the total cross section. The possibility to select one single channel of photodetachment can circumvent the issue of a slow onset at the threshold.

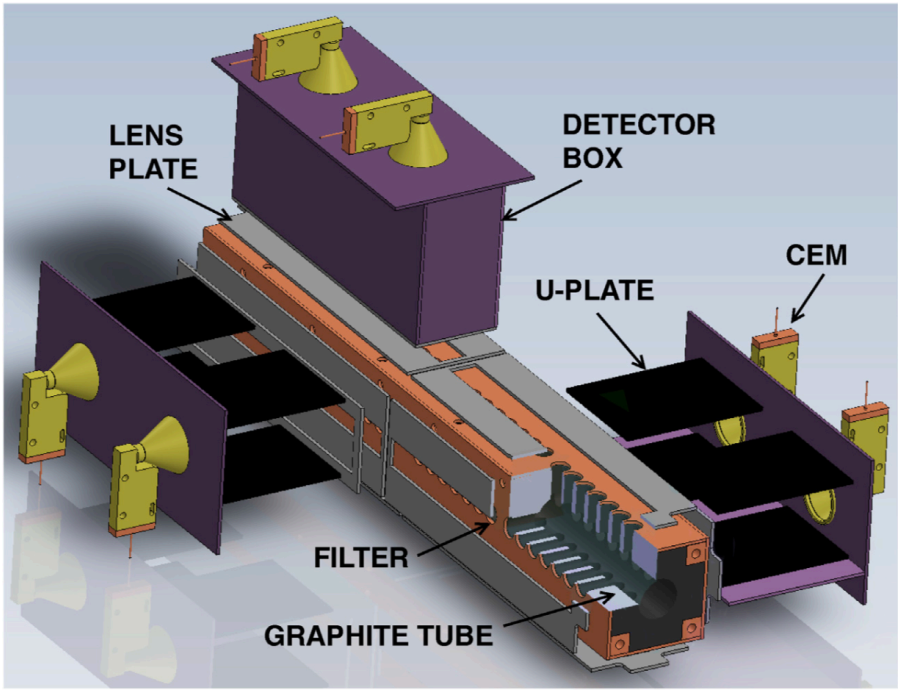

Figure 3.4: PEARLS in a 3 dimensional view with the central graphite tube in the center of the picture. Electrons exiting the tube pass through the energy filter into the detector boxes that hosts the Channel Electron Multipliers.

For this purpose a new detector called Rydberg Atom Detector for Anion Research (RADAR) has been designed. The basic layout of the detector i shown in Figure 3.5. Negative ions are interacting with one or two laser beams along a 70 cm long interaction region. Thereafter they enter a sequence of 11 concentric plates in a Field Ionizer (FI). Rydberg state excited atoms, or Rydberg atoms in short, are created by photodetachment with a photon energy sufficient to both detach the anion and excite the atom. The number of plates of the FI enables field configurations for spatially selective ionization of up to 9 sequentially neighbouring Rydberg states. Cations created from different states will be created at different positions and hence at different potentials. They will therefore be kinetic energy tagged corresponding to their atomic state. The energy tag is converted into individual trajectories in an electrostatic analyzer. The trajectories end up as spots on a Micro Channel Plate (MCP) together with an associated DLD-40 commercial position sensitive detector produced by RoentDek. Positive ions can also be produced in the interaction region due to single photon absorption (if the photon is larger than the EA and IE of the element), through multiphoton absorption or through collisions with residual gas. The energy of these positive ions are not

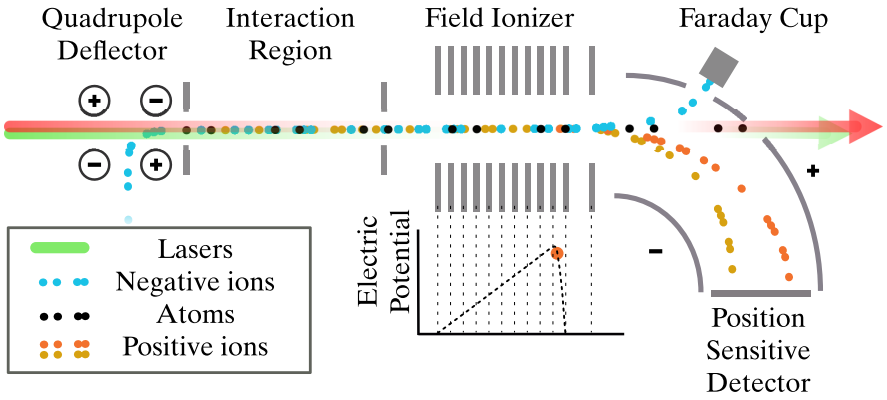

Figure 3.5: The RADAR spectrometer schematics during an operation of single channel detection for partial cross section measurements. The spectrometer consist of three segments for Rydberg atom separation. Negative ions are interacting with two laser fields in the interaction region with a collinear overlap. One for photodetachment and one for resonant excitation in order to create Rydberg atoms. Rydberg atoms are ionized and energy tagged in the field ionizer. In the last region of detection the positive ions produced in the field ionizer are spatially separated from the positive ions created in the interaction region by secondary background effects. The separation and individual detection are performed with the aid of energy analyzing bending plates and a position sensitive detector respectively.

changed during the passage through the ionizer. Hence, they will travel on a different trajectory in the electrostatic analyzer and create an individual spot on the detector. Positive ions created in a single photon absorption is of interest in experiments that aims to investigate the Wannier threshold law [58]. This type of experiment will be discussed further in Section 5. Single Rydberg state atoms may be created with a variation of the FI configuration together with a double photon excitation scheme developed by Lindahl *et al.* [49]. It enables single channel detection for partial cross section measurements as shown in the schematics of Figure 3.5.

3.2.5 Lasers

Since 1960 [117], when the report of the first laser light source was published, lasers have been an invaluable tool in many research fields. The obvious selection of light source for photodetachment are lasers due to their inherent monochromatic property, only limited by the linewidth that generally is narrow enough for high resolution spectroscopy. Since it's necessary to run energy dependent photodetachment experiments during LPT a wavelength tunable laser is a requirement. For anion

spectroscopy the wavelength regions of interest spans the whole visible spectral range as well as a few hundreds of nm into the UV and far into the IR wavelength regions. For high signal rates, the photon energy density needs to reach levels of at least $\sim 10\,\mu J$. There are several options of ns pulsed lasers that reach these densities and a few of them are available in the laboratory of GUNILLA. All of the lasers at GUNILLA are operated using a pump laser and are explained separately in the following section.

3.2.5.1 Pump Lasers

A versatile source of high intensity laser light source are lasers with the active medium of Neodymium ion doped crystal of Yttrium Aluminum Garnet, $Nd^{+}3{:}Y_3Al_5O_{12}$ or Nd:*YAG* in short. Nd:*YAG* has a wide range of absorption and emission lines that creates several options for a four level lasing scheme. The most frequently used emission line of the Nd:*YAG* is at 1064 nm, generated from flash lamp pumping. The Nd:*YAG* crystal placed in a cavity rapidly absorbs light to reach an excitation level above the lasing threshold, leading to the emission of laser radiation. The lasing is efficient enough to empty the absorbed energy within nanoseconds. Hence, the lasing threshold might be reached several times during a typical discharge flash lamp pulse of the pulse length in the microsecond range. However, a single pulse down to a $\sim 10\,ns$ pulse width is possible to create using so called Q-switching. The idea of Q-switching is to block the cavity by an electro-optical device until the energy absorption of the crystal reached its peak value. When opening the cavity, in principle all absorbed energy is released in a very short time, hence increasing the light intensity about 4 orders of magnitude. This high intensity output is ideal for frequency doubling and tripling in standard BBO based units [118]. This adds options for the laser output to the wavelengths of 532 nm and 355 nm.

For precision measurements narrow linewidths are desirable. One option is to use the so called seeding, in which a narrow laser light is introduced into the cavity from an external cw laser. At GUNILLA there are two types of pump lasers in use for second and third harmonic Nd:*YAG* emission. A 10 Hz system Quanta Ray Pro series from Spectra Physics generates 6 ns pulses with pulse energies of hundreds of mJ. The Clark-MXR, CPA-Series of variable repetition rate from 1 kHz to 10 kHz, generates output powers up to 10 W in pulses of about 10 ns. Another laser manufacturer is Edgewave that delivers the InnoSlab laser that is suitable for pumping a wide range of Chromatic conversion systems.

Systems in order to generate even shorter fixedlaser wavelengths are today realised by High Harmonic Generation (HHG) [119], [120]. By shining intense laser fields through noble gas cells it's possible to create harmonic orders over 20 [121]. A HHG system is being installed in the GUNILLA facility infrastructure. There

are other systems for HHG proposed in litterateur based on atomic negative ions [122], [123] and semiconductors [124].

3.2.5.2 Chromatic conversion system

In general fixed frequency lasers are not sufficient for atomic spectroscopy and this is also the case for LPT. However, there are several ways to convert the high intensity light of pump lasers into frequency tunable light. Some of the options are available at the GUNILLA facility and are described in the sections below. All light sources have in common a cavity with a wavelength selective diffraction grating and a partly transparent output coupler. They differ in the conversion medium and conversion specifications.

3.2.5.3 Dye Lasers

Dye lasers makes use of optical fluorescence from a liquid chemical dilution, or dye, prepared as an active medium. The Sirah Precision Scan (SPS) is tailor-made for dyes with its absorption band in one of the harmonics of a $Nd:YAG$ laser. The Sirah consists of multiple stages of dye cuvettes placed in an oscillator, a preamplifier and a main amplifier sequence. The dye of the cuvettes can easily be changed for different wavelength regions of laser emission for operation in wavelengths ranging from 375 nm to 930 nm of the SPS. Impressive spectral linewidths of sub GHz is a feature of the double grating setup of the oscillator of the SPS. The emission of the oscillator pass first a preamplifier and second the main amplifier. There are small restrictions in terms of repetition rate and pulse width for the dye systems in general, which basically inherent their features from the pump laser. At GUNILLA the SPS is pumped by a Quanta Ray Pro pump laser from Spectra Physics.

3.2.5.4 Ti:Sa Lasers

Ti:Sa is short for a Sapphire crystal (Al_2O_3) doped with Ti^{3+} titanium ions. This solid active medium has high damage threshold combined with a wide emission band in the red and IR wavelength regions. In the Ti:Sa available at the GUNILLA facility the crystal is placed in an in-house built laser with a so called z-shape cavity. It is pumped by a Clark pump laser, as described in Section 3.2.5.1. The design is based on a laser developed at Johannes Gutenberg-Universität, Mainz and ISOLDE at CERN [125], [126]. The modular setup makes use of an easy wavelength adjustment by a tiltable diffraction grating. A BBO crystal is used as an external or intracavity second harmonic generator, depending on if linewidth, power or tunability performance are preferred. As an option the cavity may be included with a wavelength restricting etalon to reach even more narrow linewidths.

3.2.5.5 OPO

An Optical Parametric Oscillation (OPO) is technically not a laser but has similar characteristics. It delivers high power coherent light from frequency conversion by higher order effects in solid state materials. These materials or crystals have relatively large non-linearity of its dielectric coupling of an exerted electric field $P = \varepsilon E + dE^2$. Here E is the electric field applied on a material with the induced polarization P with the linear electric susceptibility ε as a coupling constant. The parameter d, which in most optical systems can be neglected, becomes important when the applied field is large. The effect of the nonlinear coupling of an incoming electromagnetic wave ω_p is the probability for it to split in two outgoing waves of ω_s and ω_i. An extensive explanation of all the principles involved in this conversion is given in the doctoral thesis of J. Pearson [127]. The section below is a quick summary of the principles involved following many of the explanations found in his work.

The nonlinear frequency conversion is not at all an obvious effect but arises from quantum fluctuations called *optical parametric fluorescence*. Much like a laser facilitates "noise" or spontaneous emission to generate an avalanche of stimulated emission the parametric fluorescence can be used to create the same effect ending up in *optical parametric amplification*. The conversion is restricted in terms of energy conservation to $\omega_p = \omega_s + \omega_i$. The indices of the frequencies are chosen from the conventional naming of the incoming wave being *the pump* frequency where as the outgoing higher and lower frequencies are *the signal* and *the idler*, respectively. Due to chromatic dispersion in the crystal material the three waves in general end up out of phase for a crystal of finite length. This inhibits the amplification but can be circumvented in materials with a combination of nonlinear and birefringent properties. The birefringence introduces the possibility to adjust the dispersion by crystal rotation to keep the waves in phase. This can be summarized in the equation of all three wave vectors $\boldsymbol{k}_p = \boldsymbol{k}_s + \boldsymbol{k}_i$ in a condition called *phase matching*. This condition brings the extremely beneficial possibility to utilize the rotation of the crystal to match specific frequencies for the signal and idler. Examples of crystals available as an optical parametric amplifier, OPA, is BBO, KTP and KTA[1]. An OPA in which the pump wave is reflected back and forth in a cavity is named an optical parametric oscillator (OPO) [128]. Just as in laser cavities one can introduce frequency selective components to narrow the spectral width of the OPO emission and just as in the dye laser described in Section 3.2.5.3 the combination of an oscillator (OPO) and a subsequent amplifier (OPA) is commonly found in these laser systems.

At GUNILLA there are two commercial systems based on the OPO princi-

[1] BBO, KTP and KTA is short for Barium Borate, BaB_2O_4, Potassium titanyl phosphate $KTiOPO_4$, and Potassium titanyl arsenate, $KTiOAsO_4$ respectively.

ple. The Laser Vision custom manufactured OPO/OPA [129] deliver light from 1350 nm to 5000 nm. The MOPO:SL from the Quanta Ray series by Spectra Physics has an additional frequency doubling option (FDO) of the signal and idler output respectively which delivers laser wavelengths from 220 nm to 1800 nm. The two systems combined, can therefore cover the spectral region from UV to Mid IR.

3.3 ISOLDE

Conseil Européen pour la Recherche Nucléaire (CERN) [130] is a research facility for particle and nuclear physics located on the border between France and Switzerland just outside Geneva which for more than 60 years has been used to for research. The most famous facility is the *Large Hadron Collider* (LHC) [131]. The storage ring has a circumference of 27 km which allows it to store 7 TeV energetic proton bunches. The ring has two beam lines for counter propagating bunches and 4 interaction points with a large and complex infrastructure for detecting collisions products. The collisions create similar energetic conditions to the ones in the early universe and it's the only place in the world where this can be achieved. In order to get the TeV energy proton beam there are four preaccelerating stages [132]–[136]. Many of them were a part of CERN before the LHC and all of them have additional research facilities which make use of the high energy proton beam.

The facility with the longest history that is still operational at CERN is *Isotope mass Separator On-Line facility* (ISOLDE). Since 1967 [137] nuclear experiments have been performed at ISOLDE although it has gone through several reconstructions and extensions [138], [139]. Heavy nuclei compounds, called targets, undergo fission [140], spallation [141] and fragmentation [142] induced by the energy in the fast proton beam[1]. Daughter nuclei are created inside the proton beam targets in a highly none selective fashion, in principle covering all isotopes on the nuclear chart. However, in a specific experiment only one isotope is used. The isotopes produced in the target are ionized in a variety of different ion sources [143]. The target materials are selected for their specific properties such as release times and ion rates, thorium compounds in form of metal foils being one example. Magnetic mass separators are then used to select a specific mass of interest which can be directed to one of several research stations. Most of the research stations are in-house, such as the CRIS collaboration [144], but a large part of the beam time at ISOLDE is available for researchers applying for beam time.

The production of negative ions has until the recent years been of lower priority compared to positive. However, development and usage of surface ionizers enables negative ion extraction into the ISOLDE beam lines [145]. Another option

[1]The accelerator ring Proton Synchrotron Booster supplies up to 75 % of its total beam to ISOLDE, simultaneously being the second stage of preaccelerator for LHC

is to use an efficient methods of extracting positive ions, such as the laser source called RILIS [146]. Later a charge exchange cell [147] may be utilized in order to convert the ion beam to negative charge.

3.3.1 GANDALPH

The *Gothenburg ANion Detector for Affinity measurements by Laser Photodetachment* (GANDALPH) is an experimental system, graphically presented in Figure 3.6, which is designed for LPT studies of radioactive isotopes. At experimental

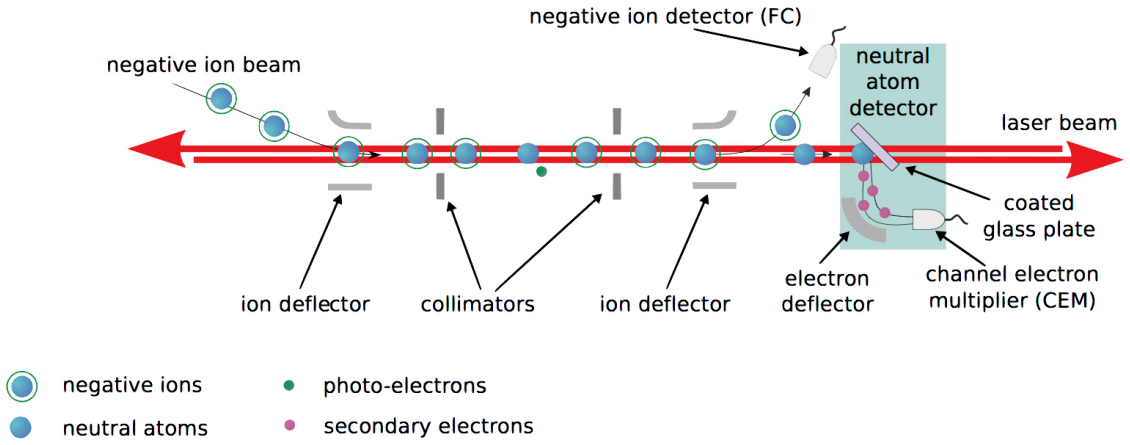

Figure 3.6: Figure from paper I showing a schematic principle of GANDALPH. A beam of negative ions is overlapped with a laser beam, arranged in either a co- or counter-propagating geometry. The neutral atoms produced in the photodetachment process impinge on a coated glass substrate where secondary electrons are created. These electrons are deflected 90° by means of an electrode where they are detected by a single channel electron multiplier. Remaining undetached ions are deflected towards a Faraday cup.

runs GANDALPH has been mounted at the GLM beam line of the General Purpose Separator (GPS) at ISOLDE. The design of GANDALPH has many similarities to the DOPPLER chamber described in Section 3.2.2. However, GANDALPH has not the interaction region tubular for doppler tuning and the ion optics are designed for ion beams above 15 keV rather than for the 6 keV beams of GUNILLA. GANDALPH, in its latest revision, also utilizes a number of new detectors for low ion rate detection, beam diagnostics as well as alpha particle detection. The increased versatility of GANDALPH is described in detail in Leimbach *et al.* [148].

4 Result

In this chapter the results of the research project I've been involved in as a Ph.D student are presented and summarized. The results are described in detail in the six appended papers.

4.1 A new design of NPD, an application of Graphene (Paper I)

As explained in previous chapters NPD:s are used for detection of the residual atom in the photodetachment process. Different versions of NPD-detectors are used at DESIREE [69], [70], [74], VERA [78], [149], CERN-ISOLDE (This work, Paper I) and at GUNILLA [150]. The target plate needs the combined properties of being transparent and conducting. It obviously needs to be transparent in order to allow laser light to pass through, and it needs to be conducting in order to avoid being charged. Prior to this work, the target plate has been made from standard glass (BK7) coated with ITO (Indium doped Tin Oxide). This has limited the photon energy ranges in LPT to below 3.7 eV due to the opacity of ITO. The work of Paper I presents a NPD with graphene coated quartz as the target plate. Benchmark experiments showed the obvious benefits of the new target material both with respect to the wavelength range and to an extremely small background emission. Full functionality is displayed in Paper I at 5.3 eV which proves a major improvement compared to the ITO coated plates. The new target material is already implemented as standard at GUNILLA and was used in the upgraded version of GANDALPH at ISOLDE-CERN in October 2018 when the electron affinty of astatine was successfully measured.

4.2 Photodetachment of radioactive iodine, towards revealing EA of astatine (Paper II)

In 2013 a collaboration between CERN, Mainz Universität and GU was formed with the ultimate goal to determine the EA of At^-. The use of ISOLDE (Section 3.3) was a necessity since all isotopes of At are radioactive. After construction of the new spectrometer GANDALPH (Section 3.3.1) and being granted beam time at ISOLDE, a first measurement was conducted in the summer of 2016. At that point the first experimental investigation of a radioactive isotope negative ion was performed where the EA of $^{128}\mathrm{I}^-$ ($t_{1/2} = 25\,\mathrm{min}$) was determined to be 3.059 052(38) eV. ^{128}I was produced in fission induced by 1.4 GeV protons striking a thorium/tantalum foil target and then extracted as singly charged negative ions at a beam energy of 20 keV. LPT with laser light produced with a $Ti{:}Sa$ laser was performed during 40 min using anti-parallel laser and ion beams. The beam time available did not allow for additional LPT with parallel alignment which would have allowed reduction of the Doppler shift to all orders (see Section 2). Instead the beam energy was determined using the well known EA of $^{127}\mathrm{I}^-$. The details on this procedure is presented in Paper II. This lead to a higher uncertainty of the EA, which prevailed in the determination of an isotope shift between the $^{128}\mathrm{I}^-$ and $^{127}\mathrm{I}^-$ isotopes.

Technical difficulties that were identified during the experiment were connected to the neutral particle detector of GANDALPH. The pressure of lower than 10^{-8} mbar diminished the background rate of collisional detached anions to a negligible level. Instead the decay of radioactive isotopes in the NPD:s glass plate constituted the main background signal that increased during the experimental beam time.

Nevertheless, the successful determination of the EA of $^{128}\mathrm{I}^-$ consitutes a major milestone in the efforts to measure the EA of astatine.

4.3 Spectroscopy on a rare element (Paper III)

A laser photodetachment threshold investigation of astatine anions, described in detail in Paper III, were performed at the radioactive beam facility ISOLDE (see Section 3.3). The spallation products of a target consisting of a Th/Ta composition were ionized by a ISOLDE-MK4 negative ion surface ionizer [145]. The ions were extracted by electrodes on 20 kV potential compared to the surface ionizer and created into an essentially monoenergetic negative ion beam. A mass separating magnet was used in order to prepare an isobaric beam of $^{211}\mathrm{At}^-$ ions that was guided to the GANDALPH spectrometer, here it was superimposed collinearly with a laser

beam. A Sirah laser using dye Coumarin 503 resolved in ethanol was pumped by the third harmonic of a 10kHz repetition Nd:YAG InnoSlab laser. The laser light power was in the range 20 mW to 30 mW in the interaction region of GANDALPH with a pulse duration of 7 ns and a linewidth of 12 GHz. The production rate of neutral astatine atoms were monitored in a neutral particle detector as the photon energy were scanned over threshold for photodetachment. The collinear overlap was performed with both parallel and anti-parallel laser and ion beams. The photon energy was scanned over the range of $h\nu$ =2.411 eV to 2.4301 eV. All instrumental noise and statistical effects of the measurement produced an uncertainty lower than the limiting uncertainty of 50 µeV from the laser linewidth. The threshold data were fitted with a nonlinear regression routine, with uncertainty weighted least squares as residuals, using an adapted version of Equation 2.22,

$$\sigma(h\nu) = a + b\sum_{F=3}^{6}(2F+1)\sqrt{h\nu - (EA + \Delta E_{hfs,F})}\Theta\left(h\nu - (EA + \Delta E_{hfs,F})\right). \tag{4.1}$$

Here, the sum runs over all possible atomic hyperfine levels of quantum number $F = 3 - 6$ with a corresponding threshold energy shift $\Delta E_{hfs,F}$ compared to the EA. The discontinuity of the channel openings is realized by the Heaviside step function Θ. The fitting parameters a and b handle the event of a static background and its relative strength compared to the photodetachment signal. The relative strengths of the different photodetachment channel were determined by the multiplicity $2F + 1$ of the final state in the atom. The fitting routine was applied to all scan data sets, both parallel and antiparallel, where a mean EA value for both laser alignments were retrieved. The geometrical mean of the two was utilized to remove all effects of the Doppler shift [109]. The electron affinity was determined to $EA(At) = 2.415\,78(7)$ eV.

Alongside the experiment a theoretical evaluation was made of the $EA(At)$ using the powerful computational software DIRAC15 [151] to perform a coupled cluster numerical method as the zeroth order Hamiltonian including relativistic coulomb interaction as well as electron correlation. Additionally perturbative contributions from higher order excitations, Breit interactions and Lamb Shift QED effects were added to end up at a final value of 2.414(16) eV, consistent with the experimental result.

The experiment of $^{128}I^-$ and $^{211}At^-$ opened up for new possibilities in atomic physics since we now will be able to study negative ions of elements heavier than bismuth, which are lacking stable isotopes. Another future project at GANDALPH, in which isotope shifts in EA's will be investigated, has been granted beam time at ISOLDE. This subject will be discussed further in Chapter 5.

4.4 New spectrometer for PAD (Paper IV)

Paper IV gives a thorough description of the principles and function of PEARLS that was introduced in Section 3.2.3. PEARLS is inspired by the design of a spectrometer used by D. Hanstorp *et al.* [103]. The central part of PEARLS is a 22 cm graphite cylinder with holes drilled in four rows, situated at 90° with respect to each other. Each row has 28 holes of 5 mm diameter. This enables a collinear alignment between interacting light beam and ion beam with simultaneous detection of outgoing electrons in the perpendicular direction. The electron detection using CEM:s covers four perpendicular directions with in total 16 CEM:s divided into two identical modules. The modular design could easily be extended for higher detection rates. Paper IV presents results from benchmark tests performed with 4 out of 8 possible CEM:s present in one out of the two modules.

Originally PEARLS was designed for PAD experiments at the Advance Light Source (ALS) synchrotron light source in Berkeley, USA [152], [153]. At ALS photon energies that can photoionize both atomic and molecular cations as well as anions are available. The design of PEARLS was optimized for detection of high kinetic energy electrons. However, for commissioning of the spectrometer, photodetachment studies of negative ions at GUNILLA, using in-house lasers, were performed. The accessibility to the experimental facilities is much higher at GUNILLA than at the ALS or any other synchrotron user facility and the lasers are sufficient to provide photoelectrons in the lower kinetic energy region if negative ions are used in the experiments.

For the lower energy region of photoelectrons the relative velocity due to the ion kinetic energy gets pronounced. Therefore the kinetic effects was characterized using the simulation software SIMION® [154]. The simulations were used as post-experimental processing in order to correct the systematic error caused by the kinematic effect and the non-zero acceptance angle. Additional channel openings above the photodetachment threshold constitute a contamination contribution to the PAD. Therefore, PEARLS has been equipped with electrodes that can be used to suppress low energy photoelectrons. The filters permit PEARLS to reach even higher energies for specific PAD channels.

The advantage of PEARLS is that the interaction volume is much larger than that obtained in a crossed beams geometry. This comes at a cost of a lower angular resolution. It can further be argued that the VMI spectrometer, which utilizes a crossed beams geometry, has the advantage of collecting all electrons emitted in the investigated process, whereas PEARLS only collects electron emitted at 0° and 90° with respect to the laser polarization. However, it is essentially the ratio of the emission at these two angles that contains the information about the asymmetry parameter. Therefore, by detecting electrons emitted at 0° and 90° one

essentially obtains the same information and signal levels as if electrons emitted into all directions are detected. Further, the modular design of PEARLS makes it possible to use multiple modules along the collinear beams in order to increased the collection rates.

4.5 Extended range of PAD Anions (Paper V)

Paper V presents a study of the angular dependence of the photoelectrons following photodetachment of P^-. Photoelectrons at 11 photon energies were detected perpendicularly with respect to the ion beam at 0°, 90°, 180° and 270°, relative to the laser polarization. For each photon energy values of the β parameter are retrieved. Uncertainties are dominated by statistical fluctuations and vary between photon energies due to the use of several different types of lasers.

At the photon energy of 3.06 eV a 180° rotation of the laser polarization were performed with 10° steps. The resulting angular dependence yielded a value of the asymmetry parameter $\beta = 0.31(4)$.

The experimentally determined β values have to be corrected for two instrumental effects. First, there is a kinematic effect since the detachment occurs in the rest frame of the moving ions while the detection of the emitted electrons occur in the laboratory frame. This effect, which is largest for small electron energies, can easily be corrected for by a transformation between the two frames. Second, there is a non zero acceptance angle for the electrons. This effect, which is smaller than the kinematic effect is estimated using a simulation using the software SIMION®. The measured values of the β parameter as a function of the photon energies shows the typical behaviour for a p-wave detachment where it starts at zero, shows a minimum reaching almost -1 whereafter it gradually increases toward an asymptotic value of 1. The experimental data is fitted to the expression.

$$\beta = \frac{2A_2\varepsilon(A_2\varepsilon - 2c)}{1 + 2A_2^2\varepsilon^2}$$

where A_2 and c are the model parameters and ε the energy above the threshold. This model [103], which is an approximation of the full Cooper-Zare formulation [62] of Equation 2.25, has been shown to be a very powerful tool in analyzing PAD data.

A non-linear regression of Equation 2.26 with $1/\sigma^2$ weights yielding an adjusted R-Squared of 98 %. The c parameter was implemented into the fit by letting the residual phase shift $d = \delta_2 - \delta_0$ represent c by the relation $c = \cos d$.

The estimated values of parameters A_2 and c are interesting to put into context with earlier results from similar experiments. The c-parameter describes the residual phase shift between the s- and d-waves of the outgoing electron, where a value

of 1 means that there is complete destructive interference between the two waves along the polarisation axis. This gives the extraordinary result that an electric field driving the electron along the polarization axes yields an electron emitted perpendicularly. By comparing with other experiments it is shown that a rather constant value for $c \approx 0.9$ is apparent for all examples of p-electron photodetachment. This is close to the earlier adopted value of 1 in mixed models [155]. Nevertheless it definitely deviate from being equal to unity as earlier assumed for pure p-detachment. The A_2 parameter scales with the size of the negative ion [103], [155]. As a consequence, this parameter varies significantly for different elements. However, it is expected to be inversely related to the electron affinity, since a larger affinity corresponds to a more tightly bound electron. It is shown in Paper V that the A_2 parameter indeed scale inversely with the electron affinity. Finally we should point out that a regression using a model with an energy dependence of the residual phase, also was applied to the data. However, the adjusted R-square showed no improvement for the alternative model.

4.6 Commissioning of photodetachment spectrometer with diverse scattering product analysis (Paper VI)

In Paper VI the functionality of the RADAR detector is demonstrated by first presenting the first experimental results and second simulations of the three modes of operation proposed in Section 3.2.4. The simulations was performed on ion trajectories using the commercial software SIMION®.

The experiment performed to demonstrate the performance of RADAR was to measure the partial photodetachment channel of Cs^-, leaving the residual atom in the $6p\ ^2P_{3/2}$ excited state. This particular state was selected since it gives an s-wave threshold which has a sharp onset. The subsequent steps of RIS with high atomic state selectivity and an efficient suppression of all competing partial photodetachment channels is demonstrated. The main features in the experiments are confirmed by the corresponding simulations. However, the experimental data reveals a few artifacts compared to the simulated detector images. First, the noise from PSD dark counts and detection of free electrons constitute a background spread over the whole detection image. Secondly a positional discrepancy of the simulated and the measured signal peaks is visible. By additional simulation the discrepancy can be equalized by reducing the voltages of the electrostatic bending plates with 10%. Alternatively, simulation with a 10% lower initial kinetic energy makes the ion beam follow the same trajectory observed in experiment. Finally, the uncertainty of the final alignment of the internal parts of the spectrometer may

create this slight inconsistency with simulation input parameters.

Nevertheless, the combination of the experiment and the simulation shows a successful commissioning of RADAR for single photodetachment channel spectroscopy. By using the Wigner threshold law, from Equation 2.21, the energy of the the channel onset was retrieved. Using known excitation energy of the $6s\,^2S_{1/2} - 6p\,^2P_{3/2}$ transition the electron affinity was determined to $EA(Cs^-) = 0.471\,612(9)$ eV.

The second mode of operation of RADAR, "Rydberg state branching ratios," is presented with a simulation of trajectories of a series of Rydberg excited atoms. Our simulations show how positive ions created from five adjacent Rydberg levels would hit the PSD with well defined separations. All other levels and background positive ions are spatially discriminated by deflecting them to position outside the PSD. A set of similar settings experiment can cover the whole range of Rydberg levels for principal numbers 13 to 50. The range is limited by the strength of the ionizing field and by overlapping detection spots from adjacent Rydberg levels on the PSD.

The last simulation of Paper VI shows compelling results for the goal of performing threshold spectroscopy of Cs^- at the double detachment limit. It is demonstrated that it is feasible to detect double detached ions along with a spatially separate background from the highly excited Rydberg atoms ($n < 50$). A certain level of background is generated from Rydberg atoms with $n > 50$. However the knowledge gained from Rydberg branching investigation as described above serves to estimate the background created by Rydberg atoms with $n > 50$. Moreover, products from ionization prior to the field ionizer will arise from competing scattering processes such as ionic collisions as well as ions colliding with rest gas particles in the chamber. These pre-ionized products will coincide at the signal spot of the detector giving a photon energy independent background.

5

Conclusion and Outlook

To summarize the scope of my thesis I will in this section make conclusion of my results and technical developments and discuss the future steps using the newly developed experimental stations.

The neutral particle detector (NPD) described in Paper I has a graphene coated quartz glass plate that opens new spectral domains in collinear LPT. The new design has all the benefits of its predecessors ITO but with improved spectral properties. It should be stressed that the limit of 230 nm or 5.4 eV in the UV wavelenth region was set by the laser used during the measurements. Hence, it's still left to investigate the true limit of the detector. The investigation would benefit from light sources stretching down to 150 nm or correspondingly 8.3 eV where the spectral transmission window for pure Quartz has a cut off. The UV region now available is one of the spectral windows of interest for instance on research on molecular isobars of penta- and diflourides. Experiments with the new NPD have already been performed where these molecules has been investigated at GUNILLA. Future mass spectrometry experiments utilizing isobaric suppression are planned in order to tests the functionality of the method at TANDEM mass spectrometers such as the VERA facility in Vienna [78]. A copy of the graphene NPD has been mounted onto GANDALPH for LPT on radioactive anions and has been used for the EA measurements of astatine that was used to obtain the results presented in Paper III.

The first commissioning of GANDALPH was performed during the work described in Paper II, with the aim to perform the very first experiment of photodetachment spectroscopy of radioactive negative ions. The successful threshold measurement of the $^{128}I^-$ ion was a milestone which demonstrated the feasibility of photodetachment of radioactive negative ion research in general. The periodic table as it's shown in Figure 2.7 has more than one fifth of its elements that has not

been experimentally investigated, and in several cases it's not yet clear if they can be produced as stable negative ions. The majority of these elements have until now been unavailable for experiments since they have no stable isotopes. With GANDALPH at ISOLDE the obstacle of radioactivity is removed and the electron affinity may be measured. The first EA to be measured of theses radioactive elements is presented in Paper III reporting the results of laser threshold spectroscopy of At^- ions. The experimentally determined $EA(At) = 2.415\,78(7)$ eV distinguishes the theoretical predictions that has been an ongoing challenge for more than a decade. Transferring the knowledge of the IEs and EAs to other research fields benefits for instance in the determination of the electron negativity, according to the Mulliken scale [156] or the prediction of chemical hardness, used in hard and soft acid theory (HSAB) [157]. Moreover examples of density functional theory (DFT) relies on the same atomic properties to calculate the chemical potential [158]. These predictive tools of chemical bindings and reactivity has been adopted over several decades and is still being pursued [159], [160].

The particular interest of astatine has been pushed by its suitability as candidate for Targeted Alpha Therapy (TAT) [161], [162]. The isotope ^{211}At has a half life of 7.2 h, a path length of 60 µm to 90 µm and an α-particle kinetic energy of 6.0 MeV to 7.5 MeV. This is a perfect match for *in vivo* radiotherapy of cancer cells [163] or more specifically in TAT. The decay products of the isotope are all stable and non toxic which minimizes the risk of internal organ damage[164]. One of the big challenges of developing the radiopharmaceutical for this type of TAT is the lack of first principle chemical studies of the rare element of astatine. Hence, characterization using atomic physical properties is of high interest [161].

Future use of GANDALPH at radioisotope facilities such as ISOLDE at CERN or IGISOL at the university of Jyväskylä has great potential for investigating the Isotopic Shift, IS, in the EA. A continuation of the earlier work on the stable isotopes $^{35}Cl^-$ and $^{37}Cl^-$ [165], now extended to include all the available radioactive isotopes of Cl^-, is now feasible. The aim of this project is to extract the specific mass shift, SMS, contribution to the total IS. The main motivation to use radioactive isotopes is that for chlorine there are at least 12 isotopes that have sufficiently long lifetimes to be investigated at an online facility, as compared with only two if the experiments are limited to stable isotopes. The SMS is a direct probe of the electron correlation between the valence electrons of the anion. Investigations of SMS is therefore of high importance in order to model the true binding mechanism of anions [89], [166], [167].

One should note that the production of ions via surface ionization is very sufficient for the halogen elements due to its relatively large EAs. There are other methods such as charge exchange from a donor gas. Future use of GANDALPH are planned at ISOLDE including the beam line of the Collinear Resonance Ionization Spectroscopy experiment, CRIS [168], [169], which uses a vapor exchange

cell to provide neutral as well as negative ion beams. This will open up for investigation of essentially any negative ion that can be form, even if their EAs are small.

The partial wave photodetachment study yield an improved value of the electron affinity of Cesium and is the first experimental result of RADAR. The selective s-wave LPT has true benefits compared regular LPT where only the primary onset behavior, determined by the ground state electron configurations of the anion and atom, can be determined. However an ordinary p-wave LPT, with impressive high accuracy, was done by Scheer *et al.* [170] retrieving an electron affinity of $EA_{\text{Scheer}}(Cs^-) = 471.64(6)\,\text{meV}$. The work of Scheer *et al.* also presents a near threshold shape resonance explained by the unbound negative ion state $6s6p\,^3P^o_1$. The currently adopted value was published in the review article of Hotorp and Lineberger and states the electron affinity to be $EA_{\text{Hotop}}(Cs^-) = 471.630(25)\,\text{meV}$ [171]. The value lacks other publication references but is confirmed in the sequel by Andersson *et al.* [172] and is discussed in Scheer *et al.* to be retrieved by partial detachment to the $6p$ level of the the atom similar to this work. An even earlier study of Cesium performed by Slater *et al.* [173] found the value $EA_{\text{Slater}}(Cs^-) = 471.5(3)\,\text{meV}$ while investigating the total photodetachment by LPT near the $6p$ channel opening and LPES with electron low pass filters for measurement of the partial photodetachment cross section. In this context the value generated from the work of Paper VI of $EA_{\text{Welander}}(Cs^-) = 471.612(9)\,\text{meV}$ is consistence with all the earlier values and with a competing level of precision.

The Partial wave LPT conducted in this work was only performed by a single geometry of co-propagating collinear ion and laser beams. Further measurement of a conter-propagating alignment has the potential to improved the precision of the measured EA by removing the dominating uncertainty of the absolute Doppler shift compensation. The uncertainty of the absolute value of the kinetic energy of the ions propagates to a final uncertainty almost one order of magnitude larger than for the unshifted value of the electron affinity. With this doppler shift uncertainty removed the laser linewidth and the energy spread of the ion beam will be the dominating sources of uncertainty. The latter is estimated from the Cesium Sputter Ion Source to be 9 meV [110] and the dye laser used for the spectroscopy measurement has a listed linewidth of 9 μeV. Hence, the limit set by these two experimental parameters has the potential to give a precision on the μeV level.

The threshold data were accumulated from one day's measurement. Data accumulated over several days would reduce the statistical noise. One could estimate an improvement factor by assuming the unbiased sample variance, $\sigma_{N_\lambda - 1}$, and the number of samples for one days measurements, N_λ at a wavelength λ to be reproducible for each day. The noise is then represented by the standard error $\sigma_{N_\lambda - 1}/\sqrt{DN_\lambda}$ and is therefore reduced by a factor $1/\sqrt{D}$, where D is the number of days of measurement. Unfortunately a vacuum breakdown and months of

trouble shooting of the ion beam of the GUNILLA facility prevented further measurements at the time of commissioning of RADAR. These things has now been resolved and the final study of the EA of Cesium will be conducted in the near future.

Another discussion brought up by Slater *et al.* that is highly relevant for partial wave LPT is the range of validity of the Wigner law. Increasingly relevant for channel openings of higher excitations where the expected energy dependence is better explained by the threshold model of O'Malley [96] with an introduced higher order term for polarizability of the parent atom. A natural extension of the experiment of Cesium would be to extend the photon energy range in order to distinguish the models for the $6p$ channel and channels of increasing excitation energy. The polarized parent atom has, during similar experiment [49], shown cases of repulsive binding potential. These findings has trigger theoretical investigation of similar effects [174] comparing contributions from the induced electrical dipole moment and a permanent electrical dipole. This special case of state interference appears for nearly degenerate states and is a perfect example of the high correlated effects in the photodetachment process and its susceptibility to the presence of other states and channel openings. Resonances due to DES are the effect of similar impact on the partial photodetachment channels.

By increasing the energy of the experiment one eventually end up in the region of high density of states, in the region of the so called Rydberg states. The features of RADAR make it possible to investigate Rydberg states and the energy dependence of the branching ratios between the same as shown by the simulations presented in Paper VI. The Rydberg state selective field ionization of RADAR creates a versatile spectrometer that can map a large range of states in a handful number of settings. The Rydberg states play an important role in the fundamental understanding of atomic theory, such as in the theory describing the polarizability of atoms [175]. The alkalies are suitable systems for investigations of photodetachment close to the double detachment and for the same reason also suitable for investigating the Rydberg channels. Their relatively low value of EA and IE adds up energies in the near visible UV spectral range such as 284 nm for Cs^- and 256 nm for K^-. This was acknowledged already in 1988 by Bae and Peterson [176] who measured the double detachment cross section of potassium over a range -70 meV to 250 meV relative to the threshold. They showed an energy dependence of the photodetachment rate showed with features corresponding to the theory of Wannier [58]. However, it showed equally good correspondence with the model of Temkin [56]. Bae and Peterson stress the fact that their background rate may be obscuring their possibility to conclusively rule out one of the models with their experiment. Nevertheless, they claim that the background of field ionized of Rydberg states are restricted to stem from those of $n > 30$.

RADAR benefits from several points of improvements compared to the equip-

ment of Bae and Peterson. First, the selectivity of RADAR aims to separate Rydberg atoms of the states $n < 50$ and the signal in order to monitor their energy dependence simultaneously. RADAR has about 20 times better vacuum and hence a drastic reduction in the collisional detachment background. The spectral wavelengths can be covered by for instance the OPO system GUNILLA, as described in Section 3.2.5. The OPO system of GUNILLA has a listed linewidth on the order of 1 cm^{-1} which provides the spectral resolution needed.

PEARLS is now a fully functional spectrometer for PAD experiments which originally was designed for synchrotron light experiments. The low photon flux of these light sources is compensated with large interaction volume due to the collinear geometry where increased signal rates compared to crossed beam geometry saves valuable beam time. The benchmark experiments presented in Paper IV shows the full capability of PEARLS as a movable spectrometer. The results of photoelectron angular spectroscopy of phosphorus extends the benchmarking to a slightly more complex system and proves PEARLS capability to investigate the full variation angular dependencies of PADs. An approximate model of PAD energy dependence derived from the more general Cooper-Zare formula provides insights in the generality of PADs from photodetached p-electrons. The c parameter of the model directly correlates with the residual phase shift between the partial waves of s and d and has great importance in PAD experiments of molecular species [177]. In these experiments it is common to use a modelling technique of sp-mixing where the same model and hence the c-parameter represents the s part of the mixing. A frequently adopted assumption has been to set the c-parameter to unity in the sp-mixing. The result of Paper V points out that a different value of $c \approx 0.9$ to be a more realistic value for the pure s part. The shift in c will subsequently lead to a shift in the mixing ratio of the molecular PAD modelling [61].

The impact of this thesis is up for the reader to judge but the conclusions can clearly be separated in two categories. I have in my work with this thesis on one hand constructed new tools of experiments with increasing possibilities for the research field of negative ions. On the other hand I have with laser spectroscopy provided fundamental atomic physical findings which are of interest within this field at the same time they are interesting for other areas of research to gain better knowledge and hopefully future breakthroughs.

Bibliography

[1] J. Warbinek, D. Leimbach, D. Lu, K. Wendt, D. J. Pegg, A. Yurgens, D. Hanstorp, and J. Welander, "A graphene-based neutral particle detector", *Appl. Phys. Lett.*, vol. 114, no. 6, p. 061 902, 2019. DOI: 10.1063/1.5080517.

[2] S. Rothe, J. Sundberg, J. Welander, K. Chrysalidis, T. D. Goodacre, V. Fedosseev, S. Fiotakis, O. Forstner, R. Heinke, K. Johnston, T. Kron, U. Köster, Y. Liu, B. Marsh, A. Ringvall-Moberg, R. E. Rossel, C. Seiffert, D. Studer, K. Wendt, and D. Hanstorp, "Laser photodetachment of radioactive $^{128}I^-$", *J. Phys. G Nucl. Part. Phys.*, vol. 44, no. 10, p. 104 003, 2017. DOI: 10.1088/1361-6471/aa80aa.

[3] D. Leimbach, J. Karls, Y. Guo, R. Ahmed, J. Ballof, L. Bengtsson, F. B. Pamies, A. Borschevsky, K. Chrysalidis, E. Eliav, D. Fedorov, V. Fedosseev, O. Forstner, N. Galland, R. F. G. Ruiz, C. Granados, R. Heinke, K. Johnston, A. Koszorus, U. Koester, M. K. Kristiansson, Y. Liu, B. Marsh, P. Molkanov, L. F. Pasteka, J. P. Ramos, E. Renault, M. Reponen, A. Ringvall-Moberg, R. E. Rossel, D. Studer, A. Vernon, J. Warbinek, J. Welander, K. Wendt, S. Wilkins, D. Hanstorp, and S. Rothe, "The electron affinity of astatine", *Nat. Commun.*, vol. 11, no. 1, p. 3824, Feb. 2020. DOI: 10.1038/s41467-020-17599-2.

[4] O. Windelius, A. Aguilar, R. C. Bilodeau, A. M. Juarez, I. Rebolledo-Salgado, D. J. Pegg, J. Rohlén, T. Castel, J. Welander, and D. Hanstorp, "A collinear angle-resolved photoelectron spectrometer", *Nucl. Instruments Methods Phys. Res. Sect. B Beam Interact. with Mater. Atoms*, vol. 410, pp. 144–152, 2017. DOI: 10.1016/j.nimb.2017.08.028.

[5] O. Windelius, J. Welander, A. Aleman, D. J. Pegg, K. V. Jayaprasad, S. Ali, and D. Hanstorp, "Photoelectron Angular Distributions in Photodetachment from P^-", 2020.

[6] J. Welander, J. E. N. Navarrete, J. Rohlén, T. Leopold, R. D. Thomas, D. J. Pegg, and D. Hanstorp, "A Field Ionizer for Photodetachment Studies of Negative Ions", 2020.

[7] B. Pullman, *The atom in the history of human thought*. Oxford University Press, USA, 2001, p. 448.

[8] H. G. Liddell, *A Greek-English lexicon*, English. New York: American Book Co., 1882.

[9] E. Rutherford, "The scattering of α and β particles by matter and the structure of the atom", *Philos. Mag. Ser. 6*, vol. 21, no. 125, pp. 669–688, 1911. DOI: 10.1080/14786440508637080.

[10] H. Geiger, "On the Scattering of the α-Particles by Matter", *Proc. R. Soc. London A*, vol. 81, no. 546, p. 174, 1908. DOI: 10.1098/rspa.1983.0054.

[11] N. H. D. Bohr, "On the constitution of atoms and molecules", *Philos. Mag. Ser. 6*, vol. 26, no. 1, pp. 1–25, 1913. DOI: 10.1080/14786441308634955.

[12] R. P. Feynman, *The Feynman lectures on physics*. Reading, Mass. : Addison-Wesley Pub. Co., c1963-1965.

[13] J. J. Thomson, "Bakerian Lecture: - Rays of positive electricity", *Proc. R. Soc. London A Math. Phys. Eng. Sci.*, vol. 89, no. 607, pp. 1–20, 1913. DOI: 10.1098/rspa.1913.0057.

[14] ——, "Chathode Rays", *Philos. Mag. Ser. 5*, vol. 44, no. 269, pp. 293–316, 1897. DOI: 10.1080/14786449708621070.

[15] J. E. Geilser and S. A. Bowhill, "Ionospheric temperatures at sunspot minimum", *J. Atmos. terrestial Phys.*, vol. 27, no. 4, pp. 457–474, 1965. DOI: 10.1016/0021-9169(65)90011-5.

[16] I. A. Krinberg and A. V. Tashcihilin, "The influence of the ionosphere-plasmasphere coupling upon the latitude variations of ionospheric parameters", *Ann. Geophys.*, vol. 36, no. 4, pp. 537–548, 1980.

[17] L. Alfonsi, A. J. Kavanagh, E. Amata, P. Cilliers, E. Correia, M. Freeman, K. Kauristie, R. Liu, J. P. Luntama, C. N. Mitchell, and G. A. Zherebtsov, "Probing the high latitude ionosphere from ground-based observations: The state of current knowledge and capabilities during IPY (2007-2009)", *J. Atmos. Solar-Terrestrial Phys.*, vol. 70, no. 18, pp. 2293–2308, 2008. DOI: 10.1016/j.jastp.2008.06.013.

[18] D. R. Hartree and W. Hartree, "Self-Consistent Field, with Exchange, for Beryllium", *Proc. R. Soc. A Math. Phys. Eng. Sci.*, vol. 150, no. 869, pp. 9–33, 1935. DOI: 10.1098/rspa.1935.0085.

[19] M. Chiani, "A chart for the energy levels of the square quantum well", pp. 1–5, 2016.

[20] R. Wildt, "Electron Affinity in Astrophysics", *Astrophys. J.*, vol. 89, p. 295, 1939. DOI: 10.1086/144048.

[21] A. R. P. Rau, "The negative ion of hydrogen", *J. Astrophys. Astron.*, vol. 17, no. 3-4, pp. 113–145, 1996. DOI: 10.1007/BF02702300.

[22] T. P. Snow and V. M. Bierbaum, "Ion chemistry in the interstellar medium", *Annu. Rev. Anal. Chem. (Palo Alto. Calif).*, vol. 1, pp. 229–259, 2008. DOI: 10.1146/annurev.anchem.1.031207.112907.

[23] T. J. Millar, C. Walsh, and T. A. Field, "Negative ions in space", *Chem. Rev.*, vol. 117, no. 3, pp. 1765–1795, 2017. DOI: 10.1021/acs.chemrev.6b00480.

[24] M. C. McCarthy, C. A. Gottlieb, H. Gupta, and P. Thaddeus, "Laboratory and Astronomical Identification of the Negative Molecular Ion C_6H^-.", *Astrophys. J. Lett.*, vol. 652, no. 2, pp. L141–L144, 2006. DOI: doi:10.1086/510238.

[25] W. D. Phillips and H. Metcalf, "Laser Deceleration of an Atomic Beam", *Phys. Rev. Lett.*, vol. 48, no. 9, pp. 596–599, Mar. 1982. DOI: 10.1103/PhysRevLett.48.596.

[26] S. Chu, L. Hollberg, J. E. Bjorkholm, A. Cable, and A. Ashkin, "Three-dimensional viscous confinement and cooling of atoms by resonance radiation pressure", *Phys. Rev. Lett.*, vol. 55, no. 1, pp. 48–51, 1985. DOI: 10.1103/PhysRevLett.55.48.

[27] A. Aspect, E. Arimondo, R. Kaiser, N. Vansteenkiste, and C. Cohen-Tannoudji, "Laser cooling below the one-photon recoil energy by velocity-selective coherent population trapping", *Phys. Rev. Lett.*, vol. 61, no. 7, pp. 826–829, 1988. DOI: 10.1103/PhysRevLett.61.826.

[28] M. H. Anderson, J. R. Ensher, M. R. Matthews, C. E. Wieman, and E. A. Cornell, "Observation of Bose-Einstein Condensation in a Dilute Atomic Vapor", *Science (80-.).*, vol. 269, no. 5221, pp. 198–201, Jul. 1995. DOI: 10.1126/science.269.5221.198.

[29] K. B. Davis, M. .-.-O. Mewes, M. R. Andrews, N. J. van Druten, D. S. Durfee, D. M. Kurn, and W. Ketterle, "Bose-Einstein Condensation in a Gas of Sodium Atoms", *Phys. Rev. Lett.*, vol. 75, no. 22, pp. 3969–3973, Nov. 1995. DOI: 10.1103/PhysRevLett.75.3969.

[30] S. Removille, R. Dubessy, B. Dubost, Q. Glorieux, T. Coudreau, S. Guibal, J.-P. Likforman, and L. Guidoni, "Trapping and cooling of Sr^+ ions: strings and large clouds", *J. Phys. B At. Mol. Opt. Phys.*, vol. 42, no. 15, p. 154 014, Jul. 2009. DOI: 10.1088/0953-4075/42/15/154014.

[31] D. J. Larson, J. C. Bergquist, J. J. Bollinger, W. M. Itano, and D. J. Wineland, "Sympathetic cooling of trapped ions: A laser-cooled two-species nonneutral ion plasma", *Phys. Rev. Lett.*, vol. 57, no. 1, pp. 70–73, Jul. 1986. DOI: 10.1103/PhysRevLett.57.70.

[32] A. Kellerbauer, A. Fischer, and U. Warring, "Measurement of the Zeeman effect in an atomic anion: Prospects for laser cooling of Os^-", *Phys. Rev. A*, vol. 89, no. 4, p. 043 430, 2014. DOI: 10.1103/PhysRevA.89.043430.

[33] C. W. Walter, N. D. Gibson, Y. G. Li, D. J. Matyas, R. M. Alton, S. E. Lou, R. L. Field, D. Hanstorp, L. Pan, and D. R. Beck, "Experimental and theoretical study of bound and quasibound states of Ce-", *Phys. Rev. A - At. Mol. Opt. Phys.*, vol. 84, no. 3, p. 032 514, 2011. DOI: 10.1103/PhysRevA.84.032514.

[34] E. Jordan, G. Cerchiari, S. Fritzsche, and A. Kellerbauer, "High-Resolution Spectroscopy on the Laser-Cooling Candidate La^-", *Phys. Rev. Lett.*, vol. 115, no. 11, p. 113 001, 2015. DOI: 10.1103/PhysRevLett.115.113001.

[35] R. Tang, R. Si, Z. Fei, X. Fu, Y. Lu, T. Brage, H. Liu, C. Chen, and C. Ning, "Candidate for Laser Cooling of a Negative Ion: High-Resolution Photoelectron Imaging of Th", *Phys. Rev. Lett.*, vol. 123, no. 20, p. 203 002, 2019. DOI: 10.1103/PhysRevLett.123.203002.

[36] P. Yzombard, M. Hamamda, S. Gerber, M. Doser, and D. Comparat, "Laser cooling of molecular anions", *Phys. Rev. Lett.*, vol. 114, no. 21, p. 213 001, 2015. DOI: 10.1103/PhysRevLett.114.213001.

[37] R. C. Fortenberry, "Theoretical electronic and rovibrational studies for anions of interest to the DIBs", *Proc. Int. Astron. Union*, vol. 9, no. S297, pp. 344–348, 2014. DOI: 10.1017/S1743921313016098.

[38] R. C. Fortenberry, "Interstellar Anions: The Role of Quantum Chemistry", *J. Phys. Chem. A*, vol. 119, no. 39, pp. 9941–9953, 2015. DOI: 10.1021/acs.jpca.5b05056.

[39] M. Ahmadi, B. X. Alves, C. J. Baker, W. Bertsche, A. Capra, C. Carruth, C. L. Cesar, M. Charlton, S. Cohen, R. Collister, S. Eriksson, A. Evans, N. Evetts, J. Fajans, T. Friesen, M. C. Fujiwara, D. R. Gill, P. Granum, J. S. Hangst, W. N. Hardy, M. E. Hayden, E. D. Hunter, C. A. Isaac, M. A. Johnson, J. M. Jones, S. A. Jones, S. Jonsell, A. Khramov, P. Knapp, L. Kurchaninov, N. Madsen, D. Maxwell, J. T. McKenna, S. Menary, J. M. Michan, T. Momose, J. J. Munich, K. Olchanski, A. Olin, P. Pusa, C. Rasmussen, F. Robicheaux, R. L. Sacramento, M. Sameed, E. Sarid, D. M. Silveira, C. So, D. M. Starko, G. Stutter, T. D. Tharp, R. I. Thompson, D. P. van der Werf, and J. S. Wurtele, "Investigation of the fine structure of antihydrogen", *Nature*, vol. 578, no. 7795, pp. 375–380, Feb. 2020. DOI: 10.1038/s41586-020-2006-5.

[40] H. Massey, *Negative Ions*, 3rd ed. CUP Archive, 1976, 1976.

[41] L. M. Branscomb and S. J. Smith, "Experimental cross section for photodetachment of electrons from H^- and D^-", *Phys. Rev.*, vol. 98, no. 4, pp. 1028–1034, 1955. DOI: 10.1103/PhysRev.98.1028.

[42] L. Branscomb and S. Smith, "Electron affinity of Atomic Oxygen", *Phys. Rev. A*, vol. 98, no. 4, p. 1127, 1955.

[43] V. T. Davis, J. Thompson, and A. Covington, "Laser photodetachment electron spectroscopy studies of heavy atomic anions", *Nucl. Instruments Methods Phys. Res. Sect. B Beam Interact. with Mater. Atoms*, vol. 241, no. 1-4, pp. 118–124, 2005. DOI: 10.1016/j.nimb.2005.07.073.

[44] D. Hanstorp, "An ion beam apparatus for collinear photodetachment experiments", *Nucl. Inst. Methods Phys. Res. B*, vol. 100, no. 1, pp. 165–175, May 1995. DOI: 10.1016/0168-583X(94)00656-3.

[45] C. Blondel, C. Delsart, and F. Dulieu, "The photodetachment microscope", *Physics (College. Park. Md).*, vol. 77, no. 18, pp. 3755–3758, 1996. DOI: 10.1103/PhysRevLett.77.3755.

[46] R. J. Peláez, C. Blondel, C. Delsart, and C. Drag, "Pulsed photodetachment microscopy and the electron affinity of iodine", *J. Phys. B At. Mol. Opt. Phys.*, vol. 42, no. 12, p. 125 001, 2009. DOI: 10.1088/0953-4075/42/12/125001.

[47] D. Bresteau, C. Drag, and C. Blondel, "Isotope shift of the electron affinity of carbon measured by photodetachment microscopy", *Phys. Rev. A*, vol. 93, no. 1, p. 013 414, 2016. DOI: 10.1103/PhysRevA.93.013414.

[48] W. Chaibi, R. J. Peláez, C. Blondel, C. Drag, and C. Delsart, "Effect of a magnetic field in photodetachment microscopy", *Eur. Phys. J. D*, vol. 58, no. 1, pp. 29–37, 2010. DOI: 10.1140/epjd/e2010-00086-7.

[49] A. O. Lindahl, J. Rohlén, H. Hultgren, I. Y. Kiyan, D. J. Pegg, C. W. Walter, and D. Hanstorp, "Threshold photodetachment in a repulsive potential", *Phys. Rev. Lett.*, vol. 108, no. 3, p. 033 004, Jan. 2012. DOI: 10.1103/PhysRevLett.108.033004.

[50] J. Rohlén, A. O. Lindahl, H. Hultgren, R. D. Thomas, D. J. Pegg, and D. Hanstorp, "Threshold behaviour in photodetachment into a final state with large negative polarizability", *EPL (Europhysics Lett.*, vol. 106, no. 5, p. 53 001, 2014. DOI: 10.1209/0295-5075/106/53001.

[51] N. Berrah, J. D. Bozek, G. Turri, G. Akerman, B. Rude, H. L. Zhou, and S. T. Manson, "K-Shell Photodetachment of He-: Experiment and Theory", *Phys. Rev. Lett.*, vol. 88, no. 9, p. 093 001, 2002. DOI: 10.1103/PhysRevLett.88.093001.

[52] N. D. Gibson, C. W. Walter, O. Zatsarinny, T. W. Gorczyca, G. D. Ackerman, J. D. Bozek, M. Martins, B. M. McLaughlin, and N. Berrah, "K-shell photodetachment from C^- Experiment and theory", *Phys. Rev. A - At. Mol. Opt. Phys.*, vol. 67, no. 3, p. 030 703, 2003. DOI: 10.1103/PhysRevA.67.030703.

[53] J. B. Greenwood, G. F. Collins, J. Pedregosa-Gutierrez, J. McKenna, A. Murphy, and J. T. Costello, "Double ionization of atomic negative ions in an intense laser field", *J. Phys. B At. Mol. Opt. Phys.*, vol. 36, no. 16, pp. L235–L240, 2003. DOI: 10.1088/0953-4075/36/16/101.

[54] B. Bergues and I. Y. Kiyan, "Two-electron photodetachment of negative ions in a strong laser field", *Phys. Rev. Lett.*, vol. 100, no. 14, p. 143 004, 2008. DOI: 10.1103/PhysRevLett.100.143004.

[55] (. R. P. Rau, "Two electrons in a coulomb potential. Double-continuum wave functions and threshold law for electron-atom ionization", *Phys. Rev. A*, vol. 4, no. 1, pp. 207–220, 1971. DOI: 10.1103/PhysRevA.4.207.

[56] A. Temkin, "Threshold law for electron-Atom impact ionization", *Phys. Rev. Lett.*, vol. 49, no. 6, pp. 365–368, 1982. DOI: 10.1103/PhysRevLett.49.365.

[57] S. Geltman, "Comment on 'multiple ionization of helium and krypton by electron impact close to threshold: Appearance energies and Wannier exponents'", *J. Phys. B At. Mol. Opt. Phys.*, vol. 37, no. 10, pp. 2221–2223, 2004. DOI: 10.1088/0953-4075/37/10/N01.

[58] G. H. Wannier, "The threshold law for single ionization of atoms or ions by electrons", *Phys. Rev.*, vol. 90, no. 5, pp. 817–825, 1953. DOI: 10.1103/PhysRev.90.817.

[59] J. B. Donahue, P. A. Gram, M. V. Hynes, R. W. Hamm, C. A. Frost, H. C. Bryant, K. B. Butterfield, D. A. Clark, and W. W. Smith, "Observation of two-electron photoionization of the H^- ion near threshold", *Phys. Rev. Lett.*, vol. 48, no. 22, pp. 1538–1541, 1982. DOI: 10.1103/PhysRevLett.48.1538.

[60] J. R. Friedman, X. Q. Guo, M. S. Lubell, and M. R. Frankel, "Reexamination of tests of the Wannier threshold law for two-electron escape", *Phys. Rev. A*, vol. 46, no. 1, pp. 652–655, 1992. DOI: 10.1103/PhysRevA.46.652.

[61] D. Khuseynov, C. C. Blackstone, L. M. Culberson, and A. Sanov, "Photoelectron angular distributions for states of any mixed character: An experiment-friendly model for atomic, molecular, and cluster anions", *J. Chem. Phys.*, vol. 141, no. 12, p. 124 312, Sep. 2014. DOI: 10.1063/1.4896241.

[62] J. Cooper and R. N. Zare, "Angular distribution of photoelectrons", *J. Chem. Phys.*, vol. 48, pp. 942–943, 1968. DOI: 10.1063/1.1668742.

[63] ——, "Erratum: Angular Distribution of Photoelectrons", *J. Chem. Phys.*, vol. 49, p. 4252, 1968. DOI: 10.1063/1.1668742.

[64] K. L. Reid, "Photoelectron angular distributions: Developments in applications to isolated molecular systems", *Mol. Phys.*, vol. 110, no. 3, pp. 131–147, 2012. DOI: 10.1080/00268976.2011.640292.

[65] R. Reichle, H. Helm, and I. Y. Kiyan, "Detailed comparison of theory and experiment of strong-field photodetachment of the negative hydrogen ion", *Phys. Rev. A - At. Mol. Opt. Phys.*, vol. 68, no. 6, p. 11, 2003. DOI: 10.1103/PhysRevA.68.063404.

[66] M. Eklund, H. Hultgren, D. Hanstorp, and I. Y. Kiyan, "Orbital alignment in atoms generated by photodetachment in a strong laser field", *Phys. Rev. A - At. Mol. Opt. Phys.*, vol. 88, no. 2, pp. 1–8, 2013. DOI: 10.1103/PhysRevA.88.023423.

[67] H. Hultgren, M. Eklund, D. Hanstorp, and I. Y. Kiyan, "Electron dynamics in the ground state of a laser-generated carbon atom", *Phys. Rev. A - At. Mol. Opt. Phys.*, vol. 87, no. 3, p. 031 404, 2013. DOI: 10.1103/PhysRevA.87.031404.

[68] Z. Luo, X. Chen, J. Li, and C. Ning, "Precision measurement of the electron affinity of niobium", *Phys. Rev. A*, vol. 93, no. 2, p. 020 501, 2016. DOI: 10.1103/PhysRevA.93.020501.

[69] H. T. Schmidt, R. D. Thomas, M. Gatchell, S. Rosén, P. Reinhed, P. Löfgren, L. Brännholm, M. Blom, M. Björkhage, E. Bäckström, J. D. Alexander, S. Leontein, D. Hanstorp, H. Zettergren, L. Liljeby, A. Källberg, A. Simonsson, F. Hellberg, S. Mannervik, M. Larsson, W. D. Geppert, K. G. Rensfelt, H. Danared, A. Paál, M. Masuda, P. Halldén, G. Andler, M. H. Stockett, T. Chen, G. Källersjö, J. Weimer, K. Hansen, H. Hartman, and H. Cederquist, "First storage of ion beams in the Double Electrostatic Ion-Ring Experiment: DESIREE", *Rev. Sci. Instrum.*, vol. 84, no. 5, p. 055 115, 2013. DOI: 10.1063/1.4807702.

[70] A. Källberg, M. Björkhage, M. Blom, E. Bäckström, H. Cederquist, O. M. Hole, M. Kaminska, S. Mannervik, R. Nascimento, P. Reinhed, S. Rosén, H. T. Schmidt, and A. Simonsson, "Commissioning of the Double Electrostatic Storage Ring", *Ipac14*, pp. 2–4, 2014.

[71] R. Von Hahn, F. Berg, K. Blaum, J. R. Crespo Lopez-Urrutia, F. Fellenberger, M. Froese, M. Grieser, C. Krantz, K. U. Kühnel, M. Lange, S. Menk, F. Laux, D. A. Orlov, R. Repnow, C. D. Schröter, A. Shornikov, T. Sieber, J. Ullrich, A. Wolf, M. Rappaport, and D. Zajfman, "The electrostatic Cryogenic Storage Ring CSR - Mechanical concept and realization", *Nucl. Instruments Methods Phys. Res. Sect. B Beam Interact. with Mater. Atoms*, vol. 269, no. 24, pp. 2871–2874, 2011. DOI: 10.1016/j.nimb.2011.04.033.

[72] A. Becker, K. Blaum, C. Breitenfeldt, F. Fellenberger, S. George, J. Göck, M. Grieser, F. Grussie, R. von Hahn, P. Herwig, J. Karthein, C. Krantz, H. Kreckel, S. Kumar, M. Lange, S. Lohmann, C. Meyer, P. M. Mishra, O. Novotný, A. O'Connor, R. Repnow, S. Schippers, C. D. Schröter, K. Spruck, D. Schwalm, L. Schweikard, X. Urbain, S. Vogel, A. Wolf, J. Goeck, M. Grieser, F. Grussie, R. von Hahn, P. Herwig, J. Karthein, C. Krantz, H. Kreckel, S. Kumar, M. Lange, S. Lohmann, C. Meyer, P. M. Mishra, O. Novotny, A. O'Connor, R. Repnow, S. Schippers, C. D. Schroeter, K. Spruck, D. Schwalm, L. Schweikard, X. Urbain, S. Vogel, and A. Wolf, "The cryogenic storage ring CSR for collision experiments with state-controlled and phase-space cooled molecular ion beams", *J. Phys. Conf. Ser.*, Journal of Physics Conference Series, vol. 635, no. 7, p. 72 059, 2015. DOI: 10.1088/1742-6596/635/7/072059.

[73] H. T. Schmidt, G. Eklund, K. C. Chartkunchand, E. K. Anderson, M. Kaminska, N. De Ruette, R. D. Thomas, M. K. Kristiansson, M. Gatchell, P. Reinhed, S. Rosén, A. Simonsson, A. Källberg, P. Löfgren, S. Mannervik, H. Zettergren, and H. Cederquist, "Rotationally Cold OH- Ions in the Cryogenic Electrostatic Ion-Beam Storage Ring DESIREE", *Phys. Rev. Lett.*, vol. 119, no. 7, p. 073 001, 2017. DOI: 10.1103/PhysRevLett.119.073001.

[74] K. C. Chartkunchand, O. M. Hole, E. Bäckström, R. F. Nascimento, M. Kaminska, V. T. Davis, P. A. Neill, R. D. Thomas, S. Mannervik, J. S. Thompson, D. Hanstorp, H. T. Schmidt, and H. Cederquist, "Measuring the $^2D_{3/2}$ Ni^- excited state lifetime in DESIREE", *J. Phys. Conf. Ser.*, vol. 635, no. 9, p. 092 142, 2015. DOI: 10.1088/1742-6596/635/9/092142.

[75] K. C. Chartkunchand, M. kaminska, E. K. Anderson, M. K. Kristiansson, G. Eklund, O. M. Hole, R. F. Nascimento, M. Blom, M. Björkhage, A. Källberg, P. Löfgren, P. Reinhed, S. Rosén, A. Simonsson, R. D. Thomas, S. Mannervik, V. T. Davis, P. A. Neill, J. S. Thompson, D. Hanstorp, H. Zettergren, H. Cederquist, and H. T. Schmidt, "Radiative lifetimes of the bound excited states of Pt^-", vol. 032501, no. 94, p. 032 501, 2018. DOI: 10.1103/PhysRevA.94.032501.

[76] P. Andersson, A. O. Lindahl, D. Hanstorp, C. C. Havener, Y. Liu, and Y. Liu, "Nearly complete isobar suppression by photodetachment", *J. Appl. Phys.*, vol. 107, no. 2, p. 026 102, 2010. DOI: 10.1063/1.3291104.

[77] M. Martschini, J. Pitters, T. Moreau, P. Andersson, O. Forstner, D. Hanstorp, J. Lachner, Y. Liu, A. Priller, P. Steier, and R. Golser, "Selective laser photodetachment of intense atomic and molecular negative ion beams with the ILIAS RFQ ion beam cooler", *Int. J. Mass Spectrom.*, vol. 415, pp. 9–17, Apr. 2017. DOI: 10.1016/j.ijms.2016.12.015.

[78] M. Martschini, P. Andersson, O. Forstner, R. Golser, D. Hanstorp, A. O. Lindahl, W. Kutschera, S. Pavetich, A. Priller, J. Rohlén, P. Steier, M. Suter, and A. Wallner, "AMS of ^{36}Cl with the VERA 3 MV tandem accelerator", *Nucl. Instruments Methods Phys. Res. Sect. B Beam Interact. with Mater. Atoms*, vol. 294, pp. 115–120, 2013. DOI: 10.1016/j.nimb.2012.01.055.

[79] T. Leopold, J. Rohlén, P. Andersson, C. Diehl, M. Eklund, O. Forstner, D. Hanstorp, H. Hultgren, P. Klason, A. O. Lindahl, and K. Wendt, "Feasibility of photodetachment isobar suppression of WF_5^- with respect to HfF_5^-", *Int. J. Mass Spectrom.*, vol. 359, no. 1, pp. 12–18, 2014. DOI: 10.1016/j.ijms.2013.12.010.

[80] R. Hemsworth, H. Decamps, J. Graceffa, B. Schunke, M. Tanaka, M. Dremel, A. Tanga, H. P. De Esch, F. Geli, J. Milnes, T. Inoue, D. Marcuzzi, P. Sonato, and P. Zaccaria, "Status of the ITER heating neutral beam system", *Nucl. Fusion*, vol. 49, no. 4, p. 045 006, 2009. DOI: 10.1088/0029-5515/49/4/045006.

[81] A. Simonin, R. Agnello, S. Bechu, J. M. Bernard, C. Blondel, J. P. Boeuf, D. Bresteau, G. Cartry, W. Chaibi, C. Drag, B. P. Duval, H. P. De Esch, G. Fubiani, I. Furno, C. Grand, P. Guittienne, A. Howling, R. Jacquier, C. Marini, and I. Morgal, "Negative ion source development for a photoneutralization based neutral beam system for future fusion reactors", *New J. Phys.*, vol. 18, no. 12, p. 125 005, 2016. DOI: 10.1088/1367-2630/18/12/125005.

[82] N. H. D. Bohr, "XXXVII. On the constitution of atoms and molecules", *Philos. Mag.*, vol. 26, no. 153, pp. 476–502, 1913. DOI: https://doi.org/10.1080/14786441308634993.

[83] ——, "LXXIII. On the constitution of atoms and molecules", *Philos. Mag. Ser. 6*, vol. 26, no. 155, pp. 857–875, 1913. DOI: https://doi.org/10.1080/14786441308635031.

[84] L. de Broglie, "XXXV. A tentative theory of light quanta", *London, Edinburgh, Dublin Philos. Mag. J. Sci.*, vol. 47, no. 278, pp. 446–458, Feb. 1924. DOI: 10.1080/14786442408634378.

[85] W. Heisenberg, "Über den anschaulichen Inhalt der quantentheoretischen Kinematik und Mechanik", *Zeitschrift für Phys.*, vol. 43, no. 3, pp. 172–198, Mar. 1927. DOI: 10.1007/BF01397280.

[86] E. Schrödinger, "An undulatory theory of the mechanics of atoms and molecules", *Phys. Rev.*, vol. 28, no. 6, pp. 1049–1070, 1926. DOI: 10.1103/PhysRev.28.1049.

[87] W. Demtröder, *Atoms, molecules and photons: An introduction to atomic-, molecular- and quantum-physics*. Springer, 2006. DOI: 10.1007/3-540-32346-5.

[88] R. Wildt, "Negative Ions of Hydrogen and the Opacity of Stellar Atmospheres", *Astrophys. J.*, vol. 90, p. 611, Nov. 1939. DOI: 10.1086/144125.

[89] T. Carette and M. R. Godefroid, "Isotope shift on the chlorine electron affinity revisited by an MCHF/CI approach", *J. Phys. B At. Mol. Opt. Phys.*, vol. 46, no. 9, p. 095 003, 2013. DOI: 10.1088/0953-4075/46/9/095003.

[90] R. Si and C. Froese-Fischer, "Electron affinities of at and its homologous elements Cl, Br, and i", *Phys. Rev. A*, vol. 98, no. 5, pp. 4–10, Nov. 2018. DOI: 10.1103/PhysRevA.98.052504.

[91] C.-N. Liu and A. F. Starace, " Photodetachment of Na– ", *Phys. Rev. A*, vol. 59, no. 5, pp. 3643–3654, 2002. DOI: 10.1103/physreva.59.3643.

[92] S. Salomonson, H. Warston, and I. Lindgren, "Many-body calculations of the electron affinity for Ca and Sr.", *Phys. Rev. Lett.*, vol. 76, no. 1, pp. 3092–3095, 1996.

[93] E. Lindroth, "Photodetachment of H^- and Li^-", *Phys. Rev. A*, vol. 52, no. 4, pp. 2737–2749, Oct. 1995. DOI: 10.1103/PhysRevA.52.2737.

[94] M. Y. Amusia, *Atomic Photoeffect*. Springer Science & Business Media, 1990, pp. 1–12. DOI: 10.1007/978-1-4757-9328-4.

[95] E. P. Wigner, "On the behavior of cross sections near thresholds", *Phys. Rev.*, vol. 73, no. 9, pp. 1002–1009, 1948. DOI: 10.1103/PhysRev.73.1002.

[96] T. F. O'Malley, "Effect of long-range final-state forces on the negative-ion photodetachment cross section near threshold", *Phys. Rev.*, vol. 137, no. 6A, pp. 1668–1672, 1965. DOI: 10.1103/PhysRev.137.A1668.

[97] R. P. Madden and K. Codling, "New autoionizing atomic energy levels in He, Ne, and Ar", *Phys. Rev. Lett.*, vol. 10, no. 12, pp. 516–518, Jun. 1963. DOI: 10.1103/PhysRevLett.10.516.

[98] H. C. Bryant, B. D. Dieterle, J. Donahue, H. Sharifian, H. Tootoonchi, D. M. Wolfe, P. A. Gram, and M. A. Yates-Williams, "Observation of resonances near 11 eV in the photodetachment cross section of the H^- ion", *Phys. Rev. Lett.*, vol. 38, no. 5, pp. 228–230, Jan. 1977. DOI: 10.1103/PhysRevLett.38.228.

[99] B. W. Shore, "Parametrization of absorption-line profiles", *Phys. Rev.*, vol. 171, no. 1, pp. 43–54, 1968. DOI: 10.1103/PhysRev.171.43.

[100] U. Fano, "Effects of configuration interaction on intensities and phase shifts", *Phys. Rev.*, vol. 124, no. 6, pp. 1866–1878, 1961. DOI: 10.1103/PhysRev.124.1866.

[101] A. O. Lindahl, J. Rohlén, H. Hultgren, I. Y. Kiyan, D. J. Pegg, C. W. Walter, and D. Hanstorp, "Experimental studies of partial photodetachment cross sections in K^- below the $K(7^2P)$ threshold", *Phys. Rev. A - At. Mol. Opt. Phys.*, vol. 85, no. 3, p. 033 415, 2012. DOI: 10.1103/PhysRevA.85.033415.

[102] A. Starace, "Photoionization of Atoms", in *Springer Handb. At. Mol. Opt. Phys.* 2006, pp. 379–390. DOI: 10.1007/978-0-387-26308-3_24.

[103] D. Hanstorp, C. Bengtsson, and D. J. Larson, "Angular distributions in photodetachment from O^-", *Phys. Rev. A*, vol. 40, no. 2, pp. 670–675, 1989. DOI: 10.1103/PhysRevA.40.670.

[104] J. Liouville, "Note sur la Théorie de la Variation des constantes arbitraires.", *J. Math. Pures Appl.*, vol. 3, no. 1, pp. 342–349, 1838.

[105] H. Bradt, S. Olbert, H. Bradt, and S. Olbert, "Liouville's Theorem", in *Astrophys. Process.* Cambridge Univesrity Press, 2008, ch. Supplement, pp. 1–29.

[106] M. Génévriez and X. Urbain, "Animated-beeam measurement of the photodetachment cross section of H^-", *Phys. Rev. A*, vol. 91, no. 3, p. 1 033 403, 2015. DOI: 10.1103/PhysRevA.91.033403.

[107] A. N. Chester, V. S. Letokhov, and S. Martellucci, *Laser science and technology*. Springer Science & Business Media, 2012, vol. 35, pp. 348–357.

[108] S. L. Kaufman, "High-resolution laser spectroscopy in fast beams", *Opt. Commun.*, vol. 17, no. 3, pp. 309–312, 1976. DOI: 10.1016/0030-4018(76)90267-4.

[109] P. Juncar, C. R. Bingham, J. A. Bounds, D. J. Pegg, H. K. Carter, R. L. Mlekodaj, and J. D. Cole, "New method to measure the relativistic doppler shift: First results and a proposal", *Phys. Rev. Lett.*, vol. 54, no. 1, pp. 11–13, 1985. DOI: 10.1103/PhysRevLett.54.11.

[110] R. Middleton, "A versatile high intensity negative ion source", *Nucl. Instruments Methods Phys. Res.*, vol. 214, no. 2, pp. 139–150, 1983. DOI: 10.1016/0167-5087(83)90580-X.

[111] J. Holzl, F. K. Schulte, and H. Wagner, *Solid Surface Physics*. Springer-Verlag, 1979, pp. 1–140. DOI: 10.1007/BFb0048918.

[112] D. R. Lide, "Electron work function of the elements", in *CRC Handb. Chem. Physics, Internet Version 2005*, 85th ed., CRC Press, Boca Raton, FL, 2005, 2005, ch. 12, pp. 124–126.

[113] J. Deiglmayr, H. Herburger, H. Saßmannshausen, P. Jansen, H. Schmutz, and F. Merkt, "Precision measurement of the ionization energy of Cs I", *Phys. Rev. A*, vol. 93, no. 1, p. 013 424, 2016. DOI: 10.1103/PhysRevA.93.013424.

[114] P. Andersson, M. Martschini, A. Priller, P. Steier, R. Golser, and O. Forstner, "Spectroscopic analysis of the blue light emitted from Middleton type cesium sputter negative ion sources", *Nucl. Instruments Methods Phys. Res. Sect. B Beam Interact. with Mater. Atoms*, vol. 295, pp. 55–60, 2013. DOI: 10.1016/j.nimb.2012.11.009.

[115] D. Hanstorp, "A secondary emission detector capable of preventing detection of the photoelectric effect induced by pulsed lasers", *Meas. Sci. Technol.*, vol. 3, no. 5, p. 523, 1992.

[116] P. F. Tavares, E. Al-Dmour, A. Andersson, M. Eriksson, M. Grabski, M. Johansson, S. C. Leemann, L. Malmgren, M. Sjöström, and S. Thorin, "Commissioning of the Max Iv Light Source 3 GeV Storage Ring", *NAPAC2016, Chicago, IL, USA*, pp. 11–15, 2016.

[117] T. H. Maiman, "Stimulated Optical Radiation in Ruby", *Nature*, vol. 187, pp. 493–494, Aug. 1960. DOI: 10.1038/187493a0.

[118] P. A. Franken, A. E. Hill, C. W. Peters, and G. Weinreich, "Generation of optical harmonics", *Phys. Rev. Lett.*, vol. 7, no. 4, pp. 118–119, 1961. DOI: 10.1103/PhysRevLett.7.118.

[119] M. Y. Kuchiev, "Ati as a source for multiply charged ion production in a laser field", *J. Phys. B At. Mol. Opt. Phys.*, vol. 28, no. 23, pp. 5093–5115, Dec. 1995. DOI: 10.1088/0953-4075/28/23/016.

[120] M. Lewenstein, P. Balcou, M. Y. Ivanov, A. L'Huillier, and P. B. Corkum, "Theory of high-harmonic generation by low-frequency laser fields", *Phys. Rev. A*, vol. 49, no. 3, pp. 2117–2132, Mar. 1994. DOI: 10.1103/PhysRevA.49.2117.

[121] P. Rudawski, C. M. Heyl, F. Brizuela, J. Schwenke, A. Persson, E. Mansten, R. Rakowski, L. Rading, F. Campi, B. Kim, P. Johnsson, and A. L'Huillier, "A high-flux high-order harmonic source", *Rev. Sci. Instrum.*, vol. 84, no. 7, p. 073 103, Jul. 2013. DOI: 10.1063/1.4812266.

[122] J. Pedregosa-Gutierrez, P. A. Orr, J. B. Greenwood, A. Murphy, J. T. Costello, K. Zrost, T. Ergler, R. Moshammer, and J. Ullrich, "Evidence for rescattering in intense, femtosecond laser interactions with a negative ion", *Phys. Rev. Lett.*, vol. 93, no. 22, p. 223 001, 2004. DOI: 10.1103/PhysRevLett.93.223001.

[123] V. N. Ostrovsky and J. B. Greenwood, "High harmonic generation by halogen anions and noble gas atoms in a laser field", *J. Phys. B At. Mol. Opt. Phys.*, vol. 38, no. 12, pp. 1867–1880, 2005. DOI: 10.1088/0953-4075/38/12/004.

[124] D. Franz, S. Kaassamani, D. Gauthier, R. Nicolas, M. Kholodtsova, L. Douillard, J.-T. Gomes, L. Lavoute, D. Gaponov, N. Ducros, S. Février, J. Biegert, L. Shi, M. Kovacev, W. Boutu, and H. Merdji, "All semiconductor enhanced high-harmonic generation from a single nanostructured cone", *Sci. Rep.*, vol. 9, no. 1, p. 5663, 2019. DOI: 10.1038/s41598-019-41642-y.

[125] S. Rothe, B. A. Marsh, C. Mattolat, V. N. Fedosseev, and K. Wendt, "A complementary laser system for ISOLDE RILIS", *J. Phys. Conf. Ser.*, vol. 312, p. 052 020, 2011. DOI: 10.1088/1742-6596/312/5/052020.

[126] S. Rothe, V. N. Fedosseev, T. Kron, B. A. Marsh, R. E. Rossel, and K. D. Wendt, "Narrow linewidth operation of the RILIS titanium: Sapphire laser at ISOLDE-CERN", *Nucl. Instruments Methods Phys. Res. Sect. B Beam Interact. with Mater. Atoms*, vol. 317, pp. 561–564, 2013. DOI: 10.1016/j.nimb.2013.08.058.

[127] J. E. Pearson, "Infrared optical parametric flourescence and parametric oscillation", PhD thesis, California Institute of Technology Pasadena, 1972.

[128] J. A. Giordmaine and R. C. Miller, "Tunable Coherent Parametric Oscillation in $LiNbO_3$ at Optical Frequencies", *Phys. Rev. Lett.*, vol. 14, no. 24, pp. 973–976, 1965. DOI: 10.1103/PhysRevLett.14.973.

[129] W. R. Bosenberg and D. R. Guyer, "Broadly tunable, single-frequency optical parametric frequency-conversion system", *J. Opt. Soc. Am. B*, vol. 10, no. 9, pp. 1716–1722, 1993. DOI: 10.1364/JOSAB.10.001716.

[130] CERN, *CERN, Home Page*, 2018. DOI: https://home.cern/.

[131] S. Myers, "Large Hadron Collider commissioning and first operation", *Philos. Trans. R. Soc. A Math. Phys. Eng. Sci.*, vol. 370, no. 1961, pp. 859–875, 2012. DOI: 10.1098/rsta.2011.0348.

[132] R. H. Stokes, J. E. Crandall, and D. A. Swenson, "Proceedings of the 1979 linear accelerator conference", *IEEE Trans. Nucl. Sci.*, vol. 26, no. May 1973, p. 3469, 1979.

[133] K. Hanke, "Past and present operation of the CERN ps booster", *Int. J. Mod. Phys. A*, vol. 28, no. 13, p. 1 330 019, 2013. DOI: 10.1142/S0217751X-13300196.

[134] E. Regenstreif, "The CERN proton synchrotron. I", *Ned. T. Natuurk*, vol. 25, pp. 117–132, 1959.

[135] ——, "The CERN proton synchrotron II", *Ned. T. Natuurk*, vol. 25, pp. 149–159, 1959.

[136] H. Schönbacher and F. Coninckx, "Doses to the CERN 450-GeV super proton synchrotron and an estimate of radiation damage", *Nucl. Inst. Methods Phys. Res. A*, vol. 288, no. 2-3, pp. 612–618, 1990. DOI: 10.1016/0168-9002(90)90160-8.

[137] B. Jonson and K. Riisager, "The ISOLDE facility", *Scholarpedia*, vol. 5, no. 7, p. 9742, 2010. DOI: 10.4249/scholarpedia.9742.

[138] F. Ames, J. Cederkäll, T. Sieber, and F. J. C. Wenander, "The REX-ISOLDE Facility: Design and Commissioning Report", CERN, Tech. Rep. September, 2005.

[139] J. A. Rodriguez, W. V. Delsolaro, W. Andreazza, J. M. Bibby, N. Bidault, E. Bravin, J. C. Broere, E. D. Cantero, R. Catherall, V. Cobham, M. Elias, E. Fadakis, P. Fernier, M. A. Fraser, F. Gerigk, K. Hanke, Y. Kadi, M. L. Benito, E. Matli, S. Sadovich, E. Siesling, D. Valuch, F. Wenander, and P. Zhang, "Beam Commissioning Of The HIE-ISOLDE Post-Accelerator", *Proc. IPAC2016*, pp. 2045–2047, 2016.

[140] L. Meitner and O. Frisch, "Desintegration of Uranium by Neutrons, a New Type of Nuclear Reaction", *Nature*, vol. 143, pp. 239–240, 1939. DOI: 10.1038/183055a0.

[141] G. J. Russell, "Spallation Physics - An Overview", *Int. Collab. Adv. Neutron Sources KEK. Tsukuba*, pp. 291–299, 1990.

[142] G. Bertsch and P. J. Siemens, "Nuclear fragmentation", *Phys. Lett. B*, vol. 126, no. 1-2, pp. 9–12, 1983. DOI: 10.1016/0370-2693(83)90004-7.

[143] U. Köster, "ISOLDE target and ion source chemistry", *Radiochim. Acta*, vol. 89, no. 11-12, pp. 749–756, 2001. DOI: 10.1524/ract.2001.89.11-12.749.

[144] T. E. Cocolios, H. H. Al Suradi, J. Billowes, I. Budin□evi□, R. P. de Groote, S. De Schepper, V. N. Fedosseev, K. T. Flanagan, S. Franchoo, R. F. Garcia Ruiz, H. Heylen, F. Le Blanc, K. M. Lynch, B. A. Marsh, P. J. R. Mason, G. Neyens, J. Papuga, T. J. Procter, M. M. Rajabali, R. E. Rossel, S. Rothe, G. S. Simpson, A. J. Smith, I. Strashnov, H. H. Stroke, D. Verney, P. M. Walker, K. D. A. Wendt, and R. T. Wood, "The Collinear Resonance Ionization Spectroscopy (CRIS) experimental setup at CERN-ISOLDE", *Nucl. Instruments Methods Phys. Res. Sect. B Beam Interact. with Mater. Atoms*, vol. 317, pp. 565–569, 2013. DOI: https://doi.org/10.1016/j.nimb.2013.05.088.

[145] B. Vosicki, T. Björnstad, L. C. Carraz, J. Heinemeier, and H. L. Ravn, "Intense beams of radioactive halogens produced by means of surface ionization", *Nucl. Instruments Methods*, vol. 186, no. 1-2, pp. 307–313, 1981. DOI: 10.1016/0029-554X(81)90918-6.

[146] S. Rothe, T. Day Goodacre, D. V. Fedorov, V. N. Fedosseev, B. A. Marsh, P. L. Molkanov, R. E. Rossel, M. D. Seliverstov, M. Veinhard, and K. D. Wendt, "Laser ion beam production at CERN-ISOLDE: New features - More possibilities", *Nucl. Instruments Methods Phys. Res. Sect. B Beam Interact. with Mater. Atoms*, vol. 376, pp. 91–96, 2016. DOI: 10.1016/j.nimb.2016.02.024.

[147] R. Neugart, J. Billowes, M. L. Bissell, K. Blaum, B. Cheal, K. T. Flanagan, G. Neyens, W. Nörtershäuser, and D. T. Yordanov, "Collinear laser spectroscopy at ISOLDE: New methods and highlights", *J. Phys. G Nucl. Part. Phys.*, vol. 44, no. 6, 2017. DOI: 10.1088/1361-6471/aa6642.

[148] D. Leimbach, S. Rothe, L. Bengtsson, A. Ringvall-Moberg, J. Sundberg, K. Wendt, and D. Hanstorp, "Upgrades of the GANDALPH photodetachment detector towards the determination of the electron affinity of astatine", *Nucl. Instruments Methods Phys. Res. Sect. B Beam Interact. with Mater. Atoms*, vol. 463, no. December 2018, pp. 277–279, 2020. DOI: 10.1016/j.nimb.2019.05.015.

[149] A. Priller, R. Golser, P. Hille, W. Kutschera, W. Rom, P. Steier, A. Wallner, and E. Wild, "First performance tests of VERA", *Nucl. Instruments Methods Phys. Res. Sect. B Beam Interact. with Mater. Atoms*, vol. 123, no. 1-4, pp. 193–198, 1997. DOI: 10.1016/S0168-583X(96)00780-X.

[150] C. Diehl, K. Wendt, A. O. Lindahl, P. Andersson, and D. Hanstorp, "Ion optical design of a collinear laser-negative ion beam apparatus", *Rev. Sci. Instrum.*, vol. 82, no. 5, p. 053 302, May 2011. DOI: 10.1063/1.3587617.

[151] B. A. Finney and K. A. Peterson, "Beyond chemical accuracy in the heavy p-block: The first ionization potentials and electron affinities of Ga-Kr, In-Xe, and Tl-Rn", *J. Chem. Phys.*, vol. 151, no. 2, p. 024 303, 2019. DOI: 10.1063/1.5110174.

[152] M. Comacchia, "The advanced light source at the Lawrence Berkeley laboratory", *Nucl. Inst. Methods Phys. Res. B*, vol. 56-57, pp. 375–378, 1988. DOI: 10.1016/0168-583X(91)96051-L.

[153] A. Jackson, "The advanced light source at the lawrence berkeley laboratory", in *Thinking*, Lawrence Berkeley National Lab. (LBNL), Berkeley, CA (United States), 1990.

[154] S. Scientific Instrument Services, *SIMION v8.1*, 2013. DOI: www.simion.com.

[155] E. R. Grumbling and A. Sanov, "Photoelectron angular distributions in negative-ion photodetachment from mixed sp states", *J. Chem. Phys.*, vol. 135, no. 16, p. 164 302, 2011. DOI: 10.1063/1.3653234.

[156] R. S. Mulliken, "A new electroaffinity scale; Together with data on valence states and on valence ionization potentials and electron affinities", *J. Chem. Phys.*, vol. 2, no. 11, pp. 782–793, 1934. DOI: 10.1063/1.1749394.

[157] R. G. Parr, R. A. Donnelly, M. Levy, and W. E. Palke, "Electronegativity: The density functional viewpoint", *J. Chem. Phys.*, vol. 68, no. 8, pp. 3801–3807, 1978. DOI: 10.1063/1.436185.

[158] R. G. Pearson, "Hard and Soft Acids and Bases", *J. Am. Chem. Soc.*, vol. 85, no. 22, pp. 3533–3539, 1963. DOI: 10.1021/ja00905a001.

[159] P. Geerlings, F. De Proft, and W. Langenaeker, "Conceptual density functional theory", *Chem. Rev.*, vol. 103, no. 5, pp. 1793–1873, 2003. DOI: 10.1021/cr990029p.

[160] P. K. Chattaraj, U. Sarkar, and D. R. Roy, "Electrophilicity index", *Chem. Rev.*, vol. 106, no. 6, pp. 2065–2091, 2006. DOI: 10.1021/cr040109f.

[161] D. S. Wilbur, "Enigmatic astatine", *Nat. Chem.*, vol. 5, no. 3, p. 246, Feb. 2013. DOI: 10.1038/nchem.1580.

[162] D. Teze, D. C. Sergentu, V. Kalichuk, J. Barbet, D. Deniaud, N. Galland, R. Maurice, and G. Montavon, "Targeted radionuclide therapy with astatine-211: Oxidative dehalogenation of astatobenzoate conjugates", *Sci. Rep.*, vol. 7, no. 1, p. 2579, 2017. DOI: 10.1038/s41598-017-02614-2.

[163] E. J. Hall, *Radiobiology for the radiologist*, 7th ed. Philadelphia: Wolters Kluwer Health/Lippincott Williams & Wilkins, 2011.

[164] D. A. Mulford, D. A. Scheinberg, and J. G. Jurcic, "The promise of targeted α-particle therapy", *J. Nucl. Med.*, vol. 46, no. 1 SUPPL. Pp. 199–205, 2005.

[165] U. Berzinsh, M. Gustafsson, D. Hanstorp, A. Klinkmüller, U. Ljundblad, and A.-M. Mårtensson-Pandrill, "Isotope shift in the electron affinity of chlorine", *Phys. Rev. A*, vol. 51, no. 1, pp. 231–238, 1995.

[166] T. Carette, C. Drag, O. Scharf, C. Blondel, C. Delsart, C. Froese Fischer, and M. Godefroid, "Isotope shift in the sulfur electron affinity: Observation and theory", *Phys. Rev. A - At. Mol. Opt. Phys.*, vol. 81, no. 4, 2010. DOI: 10.1103/PhysRevA.81.042522.

[167] T. Carette and M. R. Godefroid, "Theoretical study of the isotope effects on the detachment thresholds of Si^-", *Phys. Rev. A - At. Mol. Opt. Phys.*, vol. 89, no. 5, p. 052 513, 2014. DOI: 10.1103/PhysRevA.89.052513.

[168] M. M. Rajabali, K. M. Lynch, T. E. Cocolios, J. Billowes, M. L. Bissell, S. De Schepper, K. Dewolf, K. T. Flanagan, F. Le Blanc, B. A. Marsh, P. J. Mason, I. Matea, G. Neyens, J. Papuga, T. J. Procter, S. Rothe, G. S. Simpson, A. J. Smith, H. H. Stroke, D. Verney, P. M. Walker, K. Wendt, and R. T. Wood, "A dedicated decay-spectroscopy station for the collinear resonance ionization experiment at ISOLDE", *Nucl. Instruments Methods Phys. Res. Sect. A Accel. Spectrometers, Detect. Assoc. Equip.*, vol. 707, pp. 35–39, 2013. DOI: 10.1016/j.nima.2012.12.090.

[169] A. R. Vernon, J. Billowes, C. L. Binnersley, M. L. Bissell, T. E. Cocolios, G. J. Farooq-Smith, K. T. Flanagan, R. F. Garcia Ruiz, W. Gins, R. P. de Groote, Koszorús, K. M. Lynch, G. Neyens, C. M. Ricketts, K. D. Wendt, S. G. Wilkins, and X. F. Yang, "Simulation of the relative atomic populations of elements $1 \leq Z \leq 89$ following charge exchange tested with collinear resonance ionization spectroscopy of indium", *Spectrochim. Acta - Part B At. Spectrosc.*, vol. 153, no. December 2018, pp. 61–83, 2019. DOI: 10.1016/j.sab.2019.02.001.

[170] M. Scheer, J. Thøgersen, R. C. Bilodeau, C. A. Brodie, and H. K. Haugen, "Experimental Evidence that the $6s6p^3P_J$ States of Cs^- Are Shape Resonances", *Phys. Rev. Lett.*, vol. 80, no. 4, pp. 684–687, 1998. DOI: 10.1103/PhysRevLett.80.684.

[171] H. Hotop and W. C. Lineberger, "Binding Energies in Atomic Negative Ions: II", *J. Phys. Chem. Ref. Data*, vol. 14, no. 3, pp. 731–750, 1985. DOI: 10.1063/1.555735.

[172] T. Andersen, H. K. Haugen, and H. Hotop, "Binding Energies in Atomic Negative Ions: III", *J. Phys. Chem. Ref. Data*, vol. 28, no. 6, pp. 1511–1533, 1999. DOI: 10.1063/1.556047.

[173] J. Slater, F. H. Read, S. E. Novick, and W. C. Lineberger, "Alkali negative ions. III. Multichannel photodetachment study of Cs^- and K^-", *Phys. Rev. A*, vol. 17, no. 1, pp. 201–213, 1978. DOI: 10.1103/PhysRevA.17.201.

[174] M. T. Eiles and C. H. Greene, "Extreme Correlation and Repulsive Interactions in Highly Excited Atomic Alkali Anions", *Phys. Rev. Lett.*, vol. 121, no. 13, p. 133 401, 2018. DOI: 10.1103/PhysRevLett.121.133401.

[175] J. Mitroy, M. S. Safronova, and C. W. Clark, "Theory and applications of atomic and ionic polarizabilities", *J. Phys. B At. Mol. Opt. Phys.*, vol. 43, no. 20, p. 202 001, 2010. DOI: 10.1088/0953-4075/43/20/202001.

[176] Y. K. Bae and J. R. Peterson, "Near-threshold measurements of K^- two-electron photoionization cross sections", *Phys. Rev. A*, vol. 37, no. 9, pp. 3254–3258, 1988. DOI: 10.1103/PhysRevA.37.3254.

[177] E. R. Grumbling, K. Pichugin, R. Mabbs, and A. Sanov, "Photoelectron imaging as a quantum chemistry visualization tool", *J. Chem. Educ.*, vol. 88, no. 11, pp. 1515–1520, 2011. DOI: 10.1021/ed100177h.

Appended papers

A graphene-based neutral particle detector

Laser photodetachment of radioactive $^{128}I^{-}$

III

The electron affinity of astatine

IV

A collinear angle-resolved photoelectron spectrometer

VI

Photoelectron Angular Distributions in Photodetachment from P^-

VI

A Field Ionizer for Photodetachment Studies of Negative Ions